REPORT DOCUMENTATION PAGE	Form Approved OMB No. 0704-0188

PLEASE DO NOT RETURN YOUR FORM TO THE ABOVE ADDRESS.

1. REPORT DATE *(DD-MM-YYYY)*	2. REPORT TYPE	3. DATES COVERED *(From - To)*
01-05-2006	Final Report	06-15-2005 - 12-14-2005

4. TITLE AND SUBTITLE

Hybrid Chem/Bio Ultradense NanoDevice Sensors (HOUNDS)

5a. CONTRACT NUMBER

N/A

5b. GRANT NUMBER

FA9550-05-1-0395

5c. PROGRAM ELEMENT NUMBER

N/A

6. AUTHOR(S)

Reed, Mark A.

5d. PROJECT NUMBER

N/A

5e. TASK NUMBER

N/A

5f. WORK UNIT NUMBER

N/A

7. PERFORMING ORGANIZATION NAME(S) AND ADDRESS(ES)

Yale Univesrity
Grant and Contract Admin.
155 Whitney Ave Suite 214
New Haven, CT 06520-8337

8. PERFORMING ORGANIZATION REPORT NUMBER

N/A

9. SPONSORING/MONITORING AGENCY NAME(S) AND ADDRESS(ES)

AFOSR
4015 Wilson Blvd
Room 713
Arlington, VA 22203-1954

10. SPONSOR/MONITOR'S ACRONYM(S)

AFOSR

11. SPONSOR/MONITOR'S REPORT NUMBER(S)

AFRL-SR-AR-TR-06-0248

12. DISTRIBUTION/AVAILABILITY STATEMENT

Public distribution/availability

13. SUPPLEMENTARY NOTES

14. ABSTRACT

The report describes technical progress toward a highly sensitive and selective molecular electronic sensor system. The effort uses state-of-the-art approaches for analyte detection and sensor design. The sensor system consists of a functionalized semiconductor nanowire matrix with a combination of different receptors (that range from highly specific nucleic acid reporters to broadband simple chemical reporters). A gating scheme provides a unique advantage that selectively tunes portions of the array to specific reactions, which enhances sensitivity and selectivity. This approach challenges the limits of detectability; a semiconductor nanowire FET which could scale to single molecule detection (and high density); and ultra sensitive nucleotide switches with unique selectivity and sensitivity.

15. SUBJECT TERMS

nanowire, sensor, riboswitch

16. SECURITY CLASSIFICATION OF:			17. LIMITATION OF ABSTRACT	18. NUMBER OF PAGES	19a. NAME OF RESPONSIBLE PERSON
a. REPORT	b. ABSTRACT	c. THIS PAGE			Dr. Hugh C. DeLong
noone	none	none	NA	43	19b. TELEPHONE NUMBER *(Include area code)* (703 696-7722

Objectives

The objectives of this effort are to explore the use of a functionalized semiconductor nanowire matrix with nucleic acid reporters for chem/bio sensors. The milestones were:

- demonstrate unambiguous detection of an analyte in an aqueous environment by gating of a semiconductor nanowire
- demonstrate identification of an analyte using a functionalized nanowire process
- demonstrate nucleotide functionalization of a semiconductor nanowire.
- downselect the specific nanowires and target functionalizations

Status

All milestones listed above were achieved. The program is continuing into Phase II funding. The progress is detailed in the next section

Accomplishments/New Findings

Background

Figure 1 illustrates the basic sensor approach. Semiconductor nanowires (NW) of various types are arranged between electrodes and functionalized with one or more receptors. The binding to, or modification of, the receptor causes a change in charge on the surface of the nanowire, changing the conductivity of the nanowire. More than one receptor per nanowire can optimize sensitivity (the largest ΔQ), selectivity (specific binding), and response speed for a given device size, often competing and conflicting requirements.

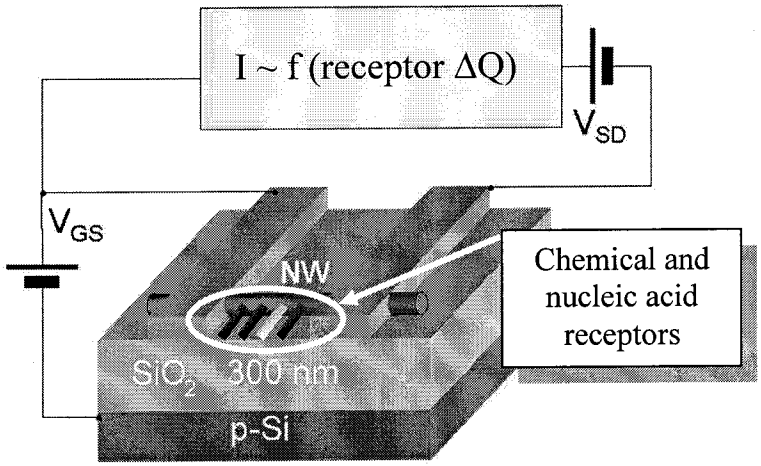

Figure 1. Gate-biased nanowire sensor

Receptors

Recent findings confirm that nucleic acids have the catalytic and kinetic sophistication to serve as molecular recognition and reporter components of next-generation biosensors. One of the team (Breaker, Yale) has developed new RNA and DNA enzymes that perform as molecular switches; specifically it is possible to tailor the activity of RNA enzymes (ribozymes) and DNA enzymes (deoxyribozymes) to respond to specific effector compounds such as small organic molecules, metal ions, and biological agents such as proteins and nucleic acids,[1-4] as shown in Figure 2. These switches also exhibit precise molecular recognition capabilities, and can identify their corresponding analyte even in the presence of closely related analogs. (Still more exotic switches have been created that trigger with protons, or that function as "binary" switches that require two effector molecules.[5])

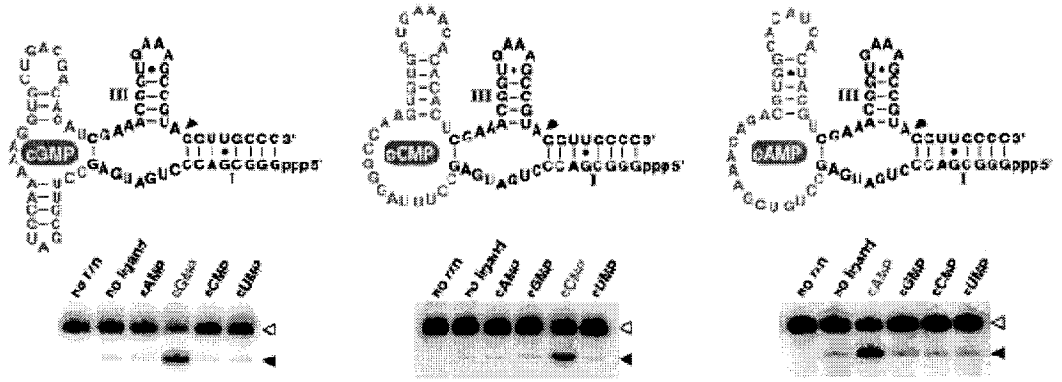

Figure 2. Structure and action of three RNA molecular switches that were isolated using allosteric selection.[6,7] Assays of 5'-^{32}P-labeled RNAs were conducted for 15 min in 500 μM of analyte. Open/filled arrowheads identify precursor/cleaved RNAs respectively.[6]

Prototypic molecular switches have been created that have dynamic ranges that span ~10^5 in analyte concentration and can be used to sense the presence of specific compounds at sub-nanomolar concentrations, even in the presence of complex chemical mixtures.[8-10] Molecular switches made of DNA, in particular, offer several distinct advantages over all other biosensor components used to date. First, DNA is approximately 100,000-fold more stable than RNA and approximately 100-fold more stable than proteins with regards to chemical (hydrolytic) destruction.[9] In addition, nucleic acid molecular switches can be created to perform with the desired catalytic and kinetic parameters under the desired analyte test conditions (in contrast to proteins, which cannot easily be reactivated upon thermal or chemical denaturation). Moreover, the DNA components of these new biochips will have a "shelf life" that is measured in *centuries* instead of weeks or months. This is an important system-level issue: most of the analytes of interest will be aqueous-based, and the sensors must operate in these conditions. However, aqueous encapsulation is problematic for long periods of time. The proposed receptors not only can be stored dry, but even if they do loose their aqueous environment they can be regenerated, making the system significantly less prone to field failure.

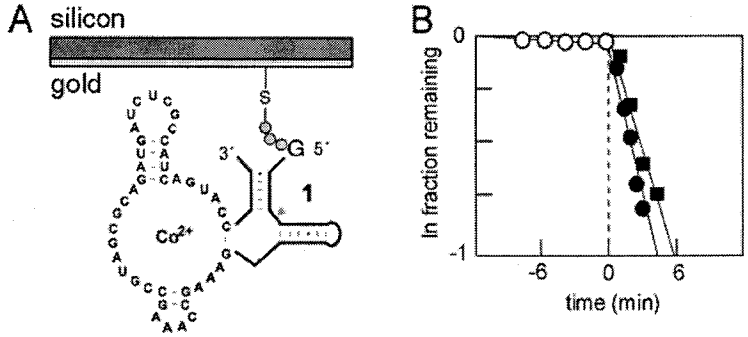

Figure 3. Demonstration of a reactive RNA biochip. (**A**) A Co^{2+} and Ni^{2+}-dependent ribozyme was immobilized using a thiol-containing RNA.[12] (**B**) Kinetics of switch function in solution (circles) or when immobilized.[10] Filled symbols identify after addition of 100 μM $NiCl_2$. The switch remains inactive prior to addition of Ni^{2+} (-6 to 0 min). The immobilized and free forms exhibit similar kinetics for RNA cleavage.

To establish that nucleic acid molecular switches can be integrated into existing microchip formats, we have demonstrated that specific RNA constructs can be immobilized on gold surfaces while retaining switch function. The immobilized RNA switch exhibits analyte-induced, reasonably fast kinetics that are nearly identical to those exhibited by the ribozyme when tested

in solution (Figure 3). Shown in Figure 4 is a multiplexed array that carries seven distinct RNA molecular switches.[10] Note that after immobilization, the RNA (or DNA) is rendered single stranded by an alkaline wash, neutralized, and stored as a dry surface until use. Application of a prepared array proceeds by rehydration/equilibration of the surface.

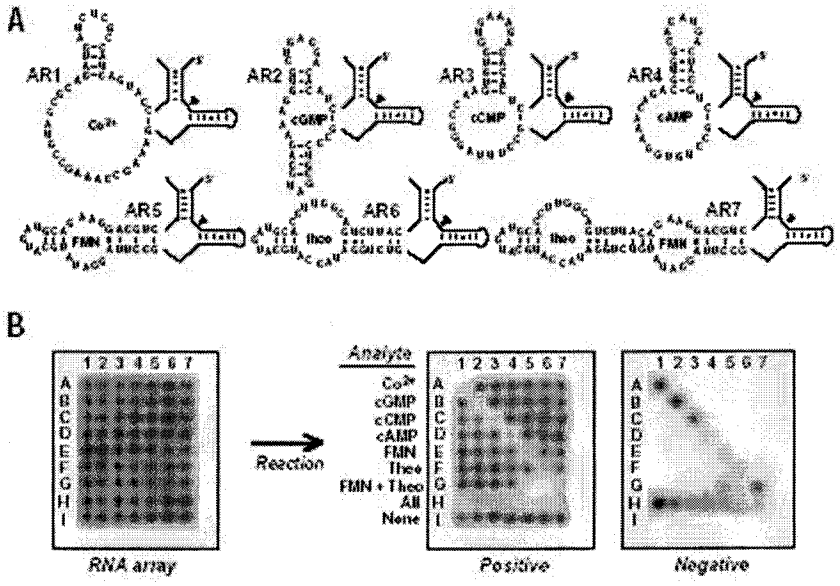

Figure 4. A prototype RNA Biochip. (**A**) Schematic representation of seven RNA molecular switches with distinct analyte specificities. Structures 1-7, respectively, are activated by the addition of divalent cobalt,[8] cyclic GMP,[6] cyclic CMP,[6] cyclic AMP,[6] flavin mononucleotide,[11] theophylline,[7] and the combined addition of flavin mononucleotide and theophylline.[5] (**B**) A prototype RNA array, where each of the rows *j* corresponds to immobilized AR*j* ribozymes. Pixels that are absent in the "positive" image identify ribozymes that self-cleave, thus liberating the radiolabeled ribozyme from the matrix and causing a loss of signal.

The engineered catalytic switches will produce very large ΔQs as the cleaved sections can have many base pairs. This produces a highly sensitive, selective functionalization. Almost any class of analyte is a candidate for detection by nucleic acid switches. Natural RNA switches are known to selectively detect proteins, amino acids, nucleobases, and coenzymes. Engineered RNA switches have been created that respond to a wide range of targets, including drug compounds (theophylline, antibiotics), signaling compounds (cAMP, cGMP, cCMP), metabolites (ATP, ADP), coenzymes (FMN), amino acids (histidine), toxic metals (cobalt, cadmium, nickel), nucleic acids, and proteins. Even pH, temperature, and UV light can be used to induce molecular switch function. It is expected that the performance characteristics of engineered nucleic acid switches can meet or even exceed those of antibodies for targets of interest.

The disadvantage is that these structures are rather large, making the 1000/sq. micron (30 nm pitch) target difficult, since this pitch is roughly the size of the nucleotide receptors. However the selectivity is so great that linearly trading off dynamic range with device size (i.e., pitch) should be very easy; i.e., if there is room for ~1 receptor at 3nm pitch, there is room for ~10 at 10nm pitch, giving a dynamic range of 10 at 100/sq. micron versus binary at 1000/sq. micron. In addition, there is a degree of selectivity that can be applied, which we will discuss in the nanowire detector section.

Are these sensors re-usable? Engineered nucleic acid switches are based on catalytic platforms that self-destruct upon exposure to the analyte. We believe we can create switches that either permit chemical regeneration of a used element, or that function without inducing self-destruction. For example in enzymes, a catalytic platform that generates a disulfide linkage upon exposure to the analyte could be used to generate signal, and reversal of this linkage can easily be achieved by brief exposure to dithiothreitol to yield a fully functional switch for reuse. Similarly, a DNA-based system could be generated by formation and reversal of an RNA phosphodiester linkage by facile chemical means. The use of DNA switches for the latter system would also dramatically increase the robustness of the system (e.g. see Figure 3).

In addition, we seek to dramatically increase the robustness of the system by creating DNA switches (e.g. see Figure 5).

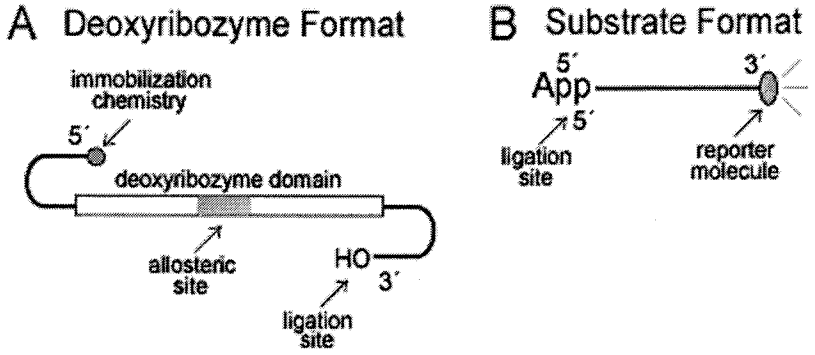

Figure 5. Configuration and chemical formats for the deoxyribozyme and substrate molecules targeted for the construction of DNA switches. (A) General architecture of the DNA ligase deoxyribozymes to be used as the reporter platform for molecular switch construction. The DNA enzyme couples DNA by a mechanism that is similar to that of the protein enzyme T4 DNA ligase. In addition, the DNA carries immobilization chemistry at its 5′ terminus, an internal analyte-binding or "allosteric site", and a 3′-terminal hydroxyl group. (B) General architecture of the substrate DNA. The substrate consists of a short DNA oligonucleotide that carries an adenyl-5′,5′-pyrophosphate group and a 3′-terminal reporter group.

Nanowire Sensors

It has been known for some time that one can potentially achieve unprecedented sensitivity in chem/bio ChemFET-like sensors by utilizing quasi-1D channels,[14] since the "bulk" channel conductivity is essentially modulated by the surface chemistry. Conventionally fabricated 1D FETs have been studied for some time, and can be sensitive enough to sense a single electron charging event.[15] To alleviate the channel fabrication challenges (at the expense of alignment), semiconducting nanowires are a better practical alternative. They have been shown to be chemical sensors and have shown an effect (however not yet unambiguously shown to be a field effect[15]) when configured as a biosensor.[16]

The FET configuration with its gate is both a crucial and a novel feature in making such a device work. By tuning the gate potential one could set the donor or acceptor levels appropriately so that charge would be either drawn into or ejected out of the nanowire when the binding occurs. This increases molecular detectability and specificity enormously converting a molecular process occurring near the surface of the nanowire into a measurable current through the nanowire. With small molecules we have already achieved detection limits ~ 10^4 molecules – a truly spectacular

potential sensing capability. With biomolecules, in which greater structural modification is expected to occur, one could hope to reduce that limit by two orders of magnitude.

The types of molecular recognition reactions that could be sensed and quantitated in this way would include: sensing of small gas-phase molecules and organics such as nerve agents, conjugate DNA and RNA oligomers or genes, substrate/enzyme interactions, protein folding events and reactions that produce protein restructuring, heme protein/small molecule interactions, antibody/antigen recognition events, solvent-induced restructuring and isomerization. Alternatively, the gate potential could be used to modify or restrict these events. For example, one can even envision creating nano-bio-motors driven by cycling the gate potential of a functionalized nanowire-based FET in such a way that the periodic isomerization of the functional molecule causes the device to propagate in a solvent in much the same manner that flagellae transport single cell animals.

Likewise, In_2O_3 nanowires are also ultra-high-performance chemical sensors for a variety of toxic species including NO_2 and NH_3. Figure 6(a) shows I-V curves recorded before and after exposing the nanowire device to 100 ppm NO_2 in Ar. While the device displayed substantial conduction before the exposure, the device was virtually insulating after exposure. Detailed analysis revealed a sensitivity (defined as the R_{after}/R_{before}) of 10^6. Figure 6(b) shows two curves recorded before and after the NH_3 exposure with the gate bias maintained at –30 V; a reduction

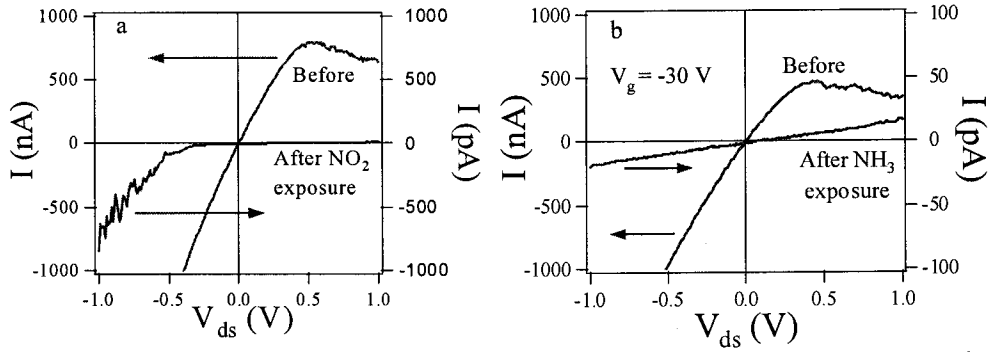

Figure 6. (a) I - V curves before and after exposure to 100 ppm NO_2. (b) I - V curves before and after exposure to 1% NH_3 with $V_g = -30$ V. The arrows inside indicate different scales.

in conductance of five orders of magnitude for $V_{ds} = -0.3$ V was obtained. Our sensitivity values (10^6 for NO_2 and 10^5 for NH_3) are significantly higher than previously reported for NO_2 and NH_3 sensing. For example, typical thin-film based chemical sensors exhibited sensitivities of 58% for NO_2 and 15% for NH_3,[17] while sensitivities less than 100 were obtained for NO_2 using SnO_2 nanobelts.[18] The maximum sensitivities obtained from semiconducting nanotubes were 1000 for NO_2 and 100 for NH_3, respectively.[19] The enhanced sensitivity with our devices is attributed to the enhanced surface-to-volume ratio, and also that the In_2O_3 nanowire surface can readily react with ambient species (as compared to the inert sidewall of carbon nanotubes). Besides the sensitivity, two other important parameters for chemical sensors are the response time and the recovery time. Detailed analysis reveals a response time (defined as the time for the conductance to change by one order of magnitude) less than 5 seconds. This is significantly better than the response time of 50 s for thin-film based semiconducting oxide sensors operating at elevated temperatures[20] upon exposure to 100 ppm NO_2. Furthermore, we have found that UV illumination can effectively help the In_2O_3 nanowire sensors recover to their initial states. Careful analysis of the response of the device under UV illumination reveals a recovery time less than 30 seconds. [21]

Progress and Accomplishments

Nucleic acid receptors

We have sought to establish methods for the rapid generation of diverse analyte sensors made from RNA or DNA molecules based on molecular switch technology. When we initiated this project, we had conducted several demonstrations that nucleic acids can perform as precision molecular sensors and switches, and had demonstrated several low-throughput methods for their generation and their application.[22,23] We have now made major advances in the high-throughput generation of RNA switches and we are continuing to examine technologies that will permit immobilization of RNA or DNA switches while retaining their 3-D shape and function. In parallel studies, we have discovered that many organisms naturally use RNA switches (called "riboswitches") to control the expression of genes. These findings validate our plan to engineer novel version of RNA switches for biosensing applications.[24]

We have had several publications on engineered RNA switches supported at least in part by this grant.[25,26] The most important new advance relates to our use of a computerized strategy to rapidly generate nucleic acid switches.[25] This publication describes our work to provide a rational design strategy for the generation of numerous different DNA- and RNA-sensing ribozymes with various ligand specificities and performance characteristics.

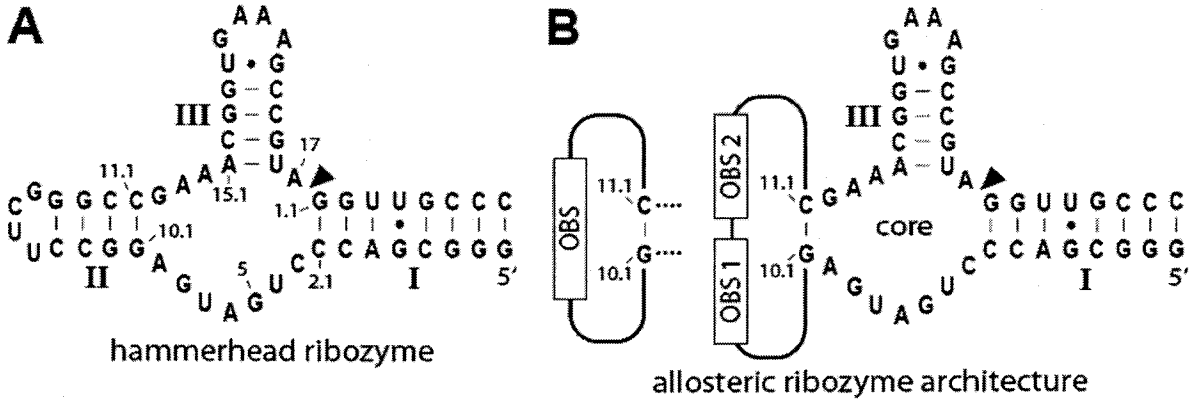

Figure 7. Engineering oligonucleotide-responsive riboswitches. The hammerhead ribozyme serves as a robust catalytic platform upon which to construct novel RNA switches. Oligonucleotide Binding Sites (OBS) can be inserted into stem II in a rational manner to create a diversity of RNA switches that respond to specific RNA or DNA targets.

Although some efforts have been made previously to employ modular rational design approaches, the resulting constructs usually are limited in ligand specificity and in functional capability. We have established a computerized design strategy that can be used to create numerous different ribozyme designs with unlimited DNA- and RNA-sensing abilities. In this study, we examine the activities of 11 ribozyme constructs that sense 11 different oligonucleotides and that exhibit various logic gate functions such as AND, OR, YES and NOT, as shown in Figures 8-10. Furthermore, we demonstrate inter-ribozyme communication between two computer-designed constructs. We proposed that such a design strategy could be used to create innumerable different sensor systems that could be used for molecular detection, molecular computing, and for the design of oligonucleotide-responsive genetic control systems.

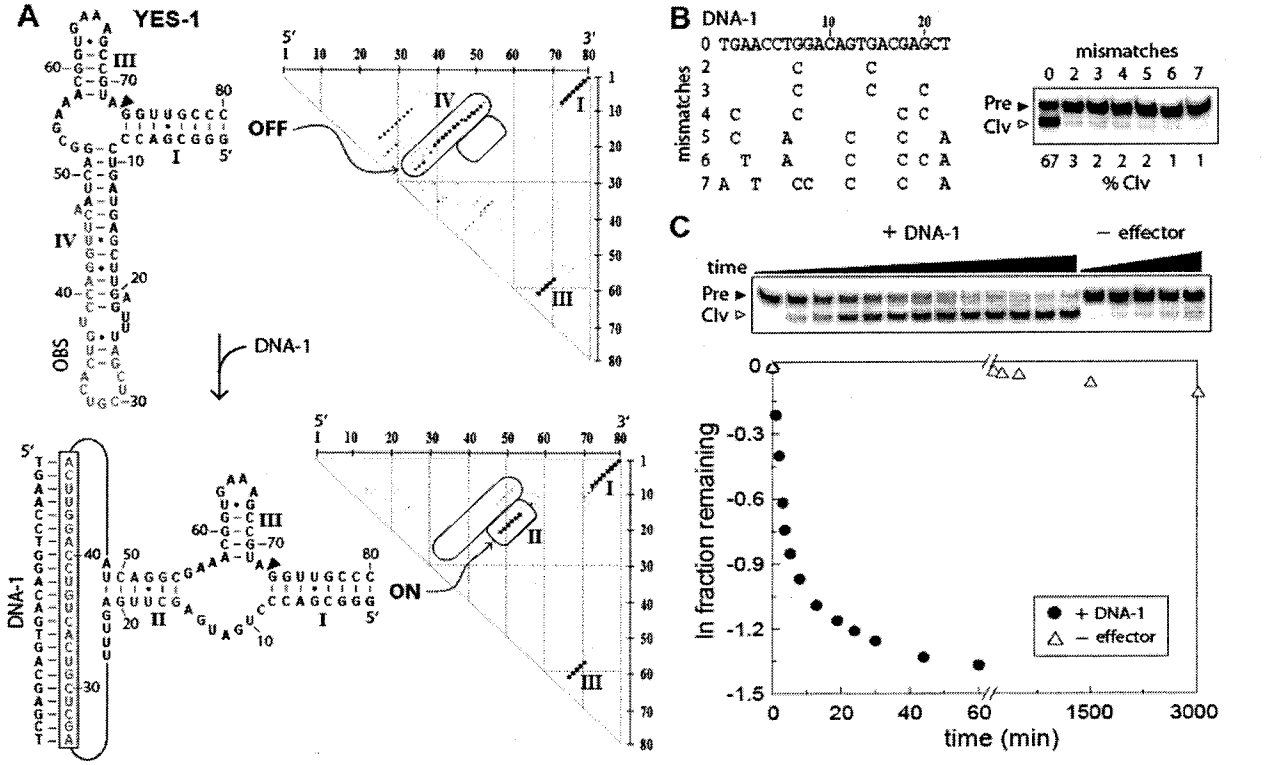

Figure 8. A riboswitch that responds to one DNA

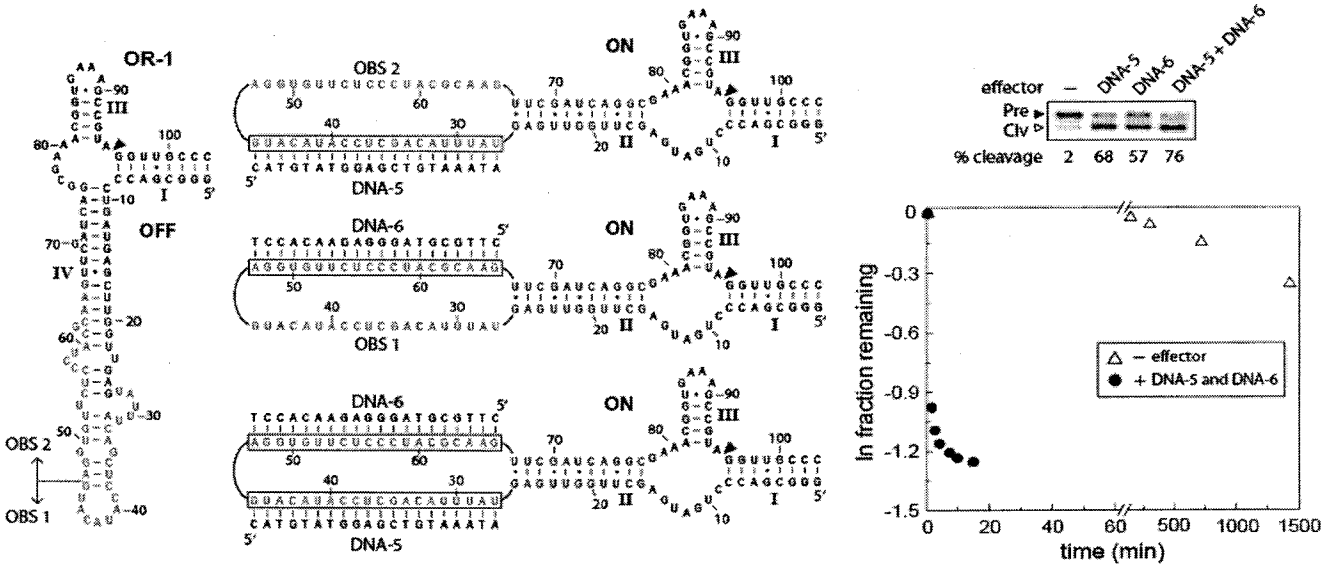

Figure 9. A riboswitch that responds to two DNAs, acting as an OR gate. The OR-1 RNA switch requires either DNA targets or both DNA targets to fire.

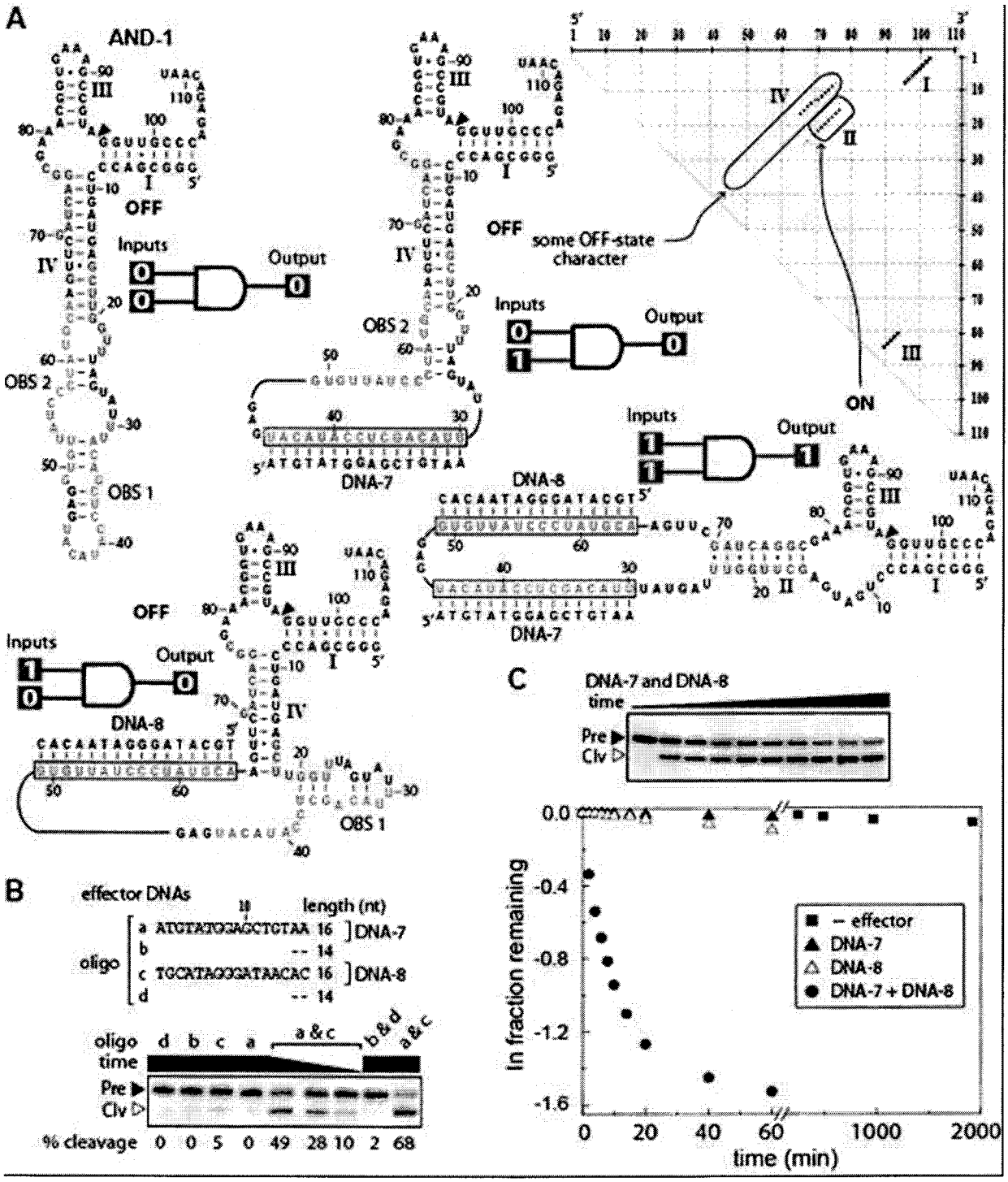

Figure 10. A riboswitch that responds to two DNAs, acting as an AND gate. The switch requires both DNA targets to fire.

Nanowires

We have investigated a number of different nanowire approaches, especially the III-nitride system due to the ease of fabrication, and the high field transport properties. This has resulted in a number of publications on the fabrication and characterization of semiconducting nanowires.[27-30] In particular, we compared unoptimized versus optimized growth conditions, and found that even with the most optimized conditions, the GaN nanowires are insufficient for sensors.

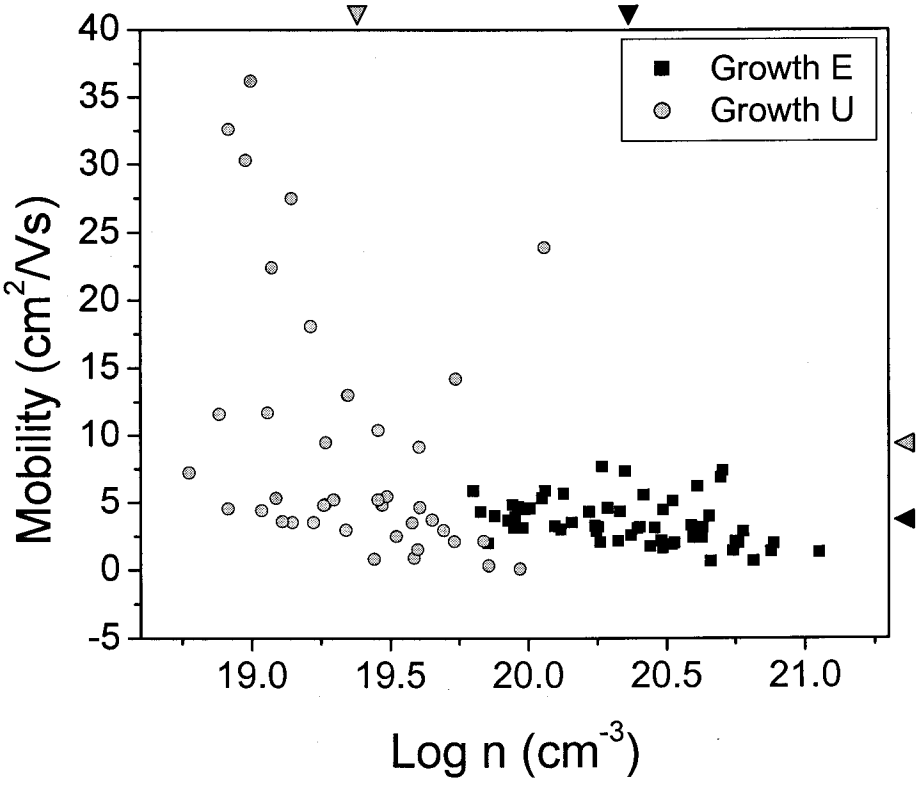

Figure 11. Plot of mobility vs. log *n* for a sample with optimized growth conditions (U) versus the original sample grown with non-optimized conditions (E). The average mobility for U is 9.12 ± 1.56 cm^2/Vs (versus 3.54 ± 0.28 cm^2/Vs for E) and the mean log carrier density is 19.39 ± 0.05 cm^{-3} (versus 20.36 ± 0.03 cm^{-3}). The mobilities and carrier concentrations are each significantly different at the 99.9% CL with $t = 4.48$, $p = 2.04 \times 10^{-5}$ and $t = 15.58$, $p = 2.87 \times 10^{-28}$, respectively.

A critical shortcoming of current surface functionalization schemes is their inability to selectively coat patterned substrates at micron and nanometer scales. This limitation prevents localized deposition of macromolecules at high densities, thereby restricting the versatility of the surface. A new approach for functionalizing lithographically patterned substrates that eliminates the need for alignment and, thus, is scalable to any dimension was achieved under this grant. We show, for the first time, that electropolymerization of derivatized phenols can functionalize patterned surfaces with amine, aldehyde, and carboxylic acid groups, and demonstrate that these derivatized groups can covalently bind molecular targets, including proteins and DNA. With this approach, electrically conducting and semiconducting materials in any lithographically realizable geometry can be selectively functionalized, allowing for the sequential deposition of a myriad of

chemical or biochemical species of interest at high density to a surface with minimal cross-contamination.

A:

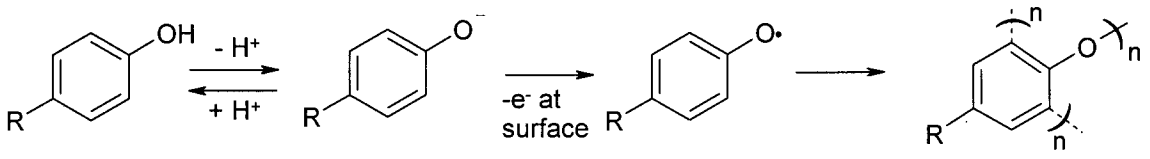

B C

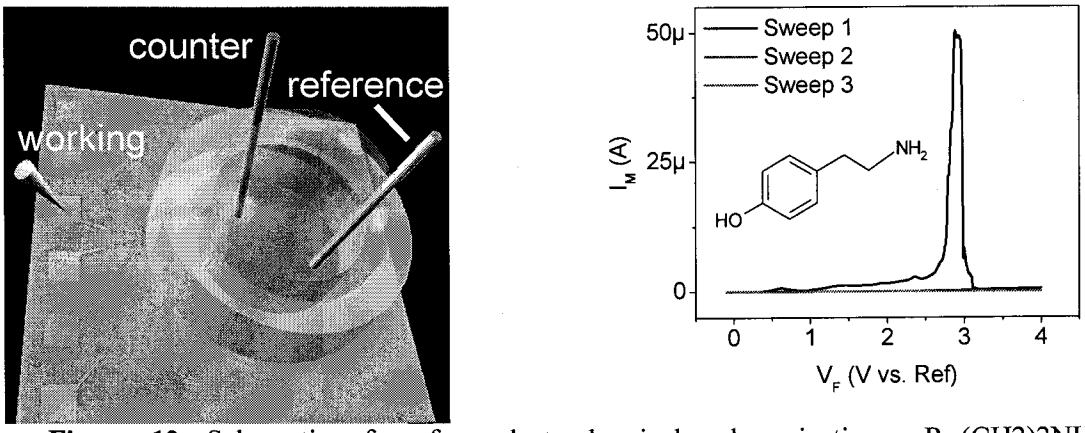

Figure 12. Schematic of surface electrochemical polymerization. R=(CH2)2NH2, CHO, CH2COOH for tyramine, 4-hydroxybenzaldehyde, and 4-hydroxyphenylacetic acid, respectively; B. Schematic (not to scale) of an electrochemical cell defined by a PDMS gasket on a patterned ITO-on-glass substrate; C. Cyclic voltammogram of the electropolymerization of tyramine (inset) on a single patterned ITO lead on a glass substrate.

To demonstrate this technique, we derivatized each of the three leads sequentially with different functional groups and then conjugated different moieties onto each group. First, the outermost lead was functionalized with amine (as described previously) and treated with a blue, amine-reactive fluorophore. Second, the innermost electrode was functionalized with aldehyde by 4-hydroxybenzaldehyde electrodeposition, followed by binding of a green, aldehyde-reactive fluorophore. After quenching remaining aldehyde groups with hydrazine, the middle lead was functionalized with carboxylic acid by 4-hydroxyphenylacetic acid electrodeposition. A red, carboxylic acid-reactive fluorophore was subsequently conjugated to the surface and the sample was then imaged; the fluorescence micrograph is shown in Fig. 3A and the localization of each of the three fluorophores is apparent. The fluorescence intensity plot demonstrates the absence of cross-functionalization interaction. These results are in press. 30

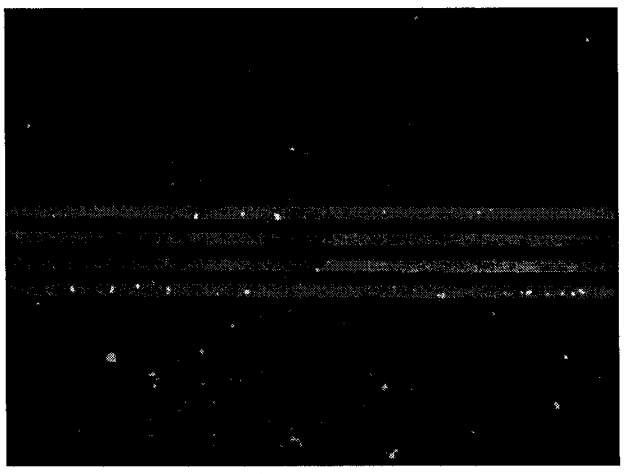

Figure 13. Multiple-fluorescence image of a central part of the lead pattern for a sample treated as follows: polytyramine was deposited on the outermost lead and the chip was subsequently treated with a blue, amine-reactive fluorophore. Poly-4-hydroxybenzene was then deposited on the innermost lead, followed by chip treatment with a green, aldehyde-reactive fluorophore. Free aldehyde groups were then quenched. Lastly, poly-4-hydroxyphenylacetic acid was deposited on the middle lead and the chip was treated a red, carboxylic acid-reactive fluorophore.

Additionally, we have demonstrated a strategy to selectively functionalize an array of nanowire (NW) biosensors with different probe molecules. In this approach we coat In_2O_3 NWs with a material that is comparatively inert in its resting form, but is activated toward chemical reactions by oxidation. Thus a given NW can be "turned-on" for binding. We demonstrated this process with a fluorescence based sensor for DNA. The procedure followed here is shown in Figure 14. Some of the NWs within a large array were biased to oxidize their surface coatings. The array is then treated with a thiol terminated DNA, which binds only to the oxidized regions. When exposed to its complimentary strand, bearing a fluorescent label, a duplex is formed and that region of the substrate is fluorescent. The thiol terminated DNA does not bid to the unoxidized regions. Using this approach we can selectively coat a specific device with a desired antibody, antigen, aptamer or other analyte binding agent, converting one or more nanowire devices within a give array into an independent sensor. This can be repeated to make multiplexed sensors.

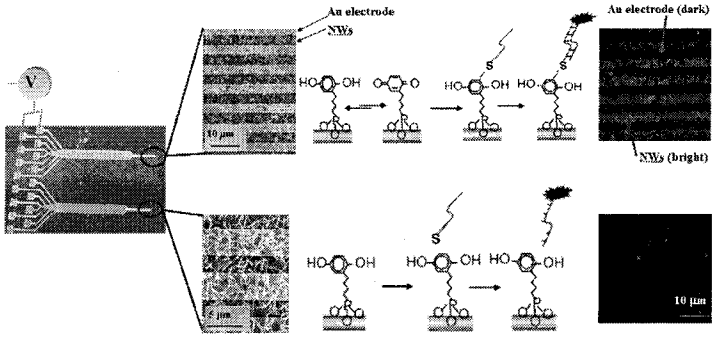

Figure 14: Outline of the strategy used to selective functionalize an array of In_2O_3 NW-based devices by electrochemically activating their surfaces and then immobilizing single-strand DNA.

In addition, we have successfully demonstrated complementary detection of prostate-specific antigen (PSA) using n-type In_2O_3 nanowires and p-type carbon nanotubes. As shown in Fig. 15, our innovation involves developing an approach to covalently attach antibodies to In_2O_3 NW surfaces via the onsite surface synthesis of phosphonic acid-succinylimide ester. Electronic measurements under dry conditions revealed complementary response for In_2O_3 NW and SWNT devices after the binding of PSA. Real time detection in solution has also been demonstrated for PSA down to 5 ng/mL, a benchmark concentration significant for clinical diagnosis of prostate cancer, which is the most frequently diagnosed cancer.

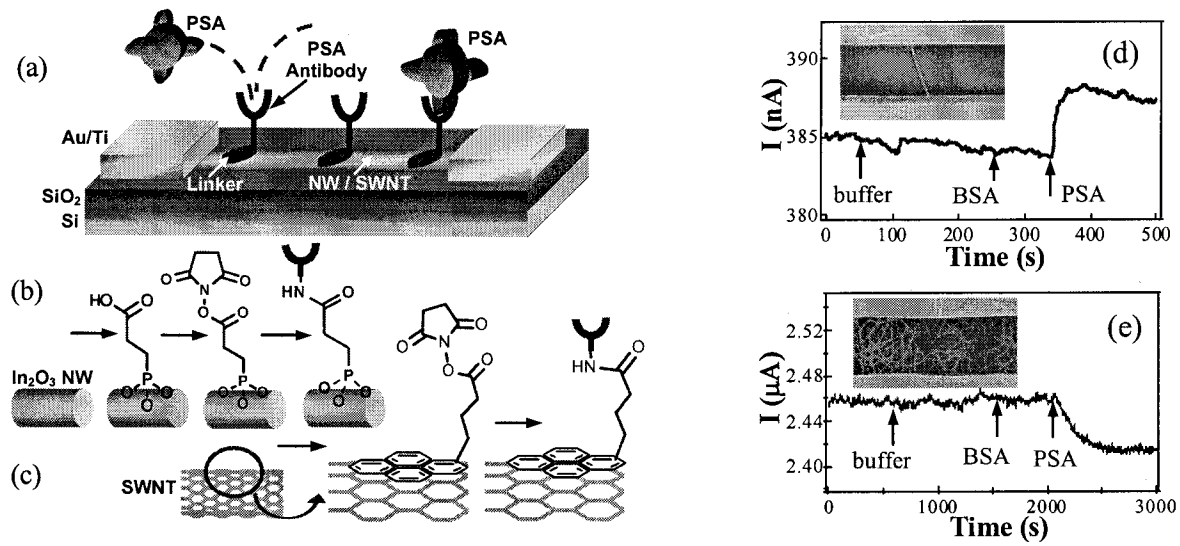

Figure 15. (a) Schematic diagram of the PSA nanobiosensors. (b) Reaction sequence for the modification of In_2O_3 NW (c) Reaction sequence for the modification of SWNT. Current recorded over time for an individual In_2O_3 NW device (d, V_{ds} = 100 mV) and a SWNT mat device (e, V_{ds} = 5 mV) while sequentially exposing the devices to buffer, BSA and PSA. Insets: SEM images of respective devices.

References

1. Soukup, G. A.; Breaker, R. R. (1999) *Trends Biotechnol.* **17**, 469-476.
2. Marshall, K. A.; Ellington, A. D. (1999) *Nat. Struct. Biol.* **6**, 992-994.
3. Soukup, G. A.; Breaker, R. R. (2000) In *Ribozymes: Biology and Biotechnology*. Edited by Gaur, R. K., Krupp, G. Natick, MA: Eaton Publishing.
4. Soukup, G. A.; Breaker, R. R. (2000) *Curr. Opin. Struct. Biol.* **10**, 318-325.
5. Jose, A.; Soukup, G. A.; Breaker, R. R. (2001) *Nucleic Acids Res.* **29**, 1631-1637.
6. Koizumi, M.; Soukup, G. A.; Kerr, J. Q.; Breaker, R. R. (1999) *Nat. Struct. Biol.* **6,** 1062-1071.
7. Soukup, G. A.; Emilsson, G. A. M.; Breaker, R. R. (2000) *J. Mol. Biol.* **298**, 623-632.
8. Zivartz, M.; Liu, Y.; Breaker, R. R. (unpublished data).
9. Li, Y. F.; Breaker, R. R. (1999) *J. Am. Chem. Soc.* **121**, 5364-5372.
10. Seetharaman, S.; Zivartz, M.; Sudarsan, N.; Breaker, R. R. (2001) *Nat. Biotechnol.* **19**, 336-341.
11. Soukup, G. A.; Breaker, R. R. (1999) *Proc. Natl. Acad. Sci. USA* **96**, 3584-3589.
12. Herne, T. M.; Tarlov, M. J. (1997) *J. Am. Chem. Soc.* **119**, 8916-8920.
13. Zhu, H.; Klemic, J.; Chang, S; Bertone, P.; Casamayor, A.; Klemic, K.; Smith, D.; Gerstein, M.; Reed, M. A.; Snyder, M. (2000) *Nat. Genetics* **26**, 283-289.
14. Ralls, K. S.; Skocpol, W. J.; Jackel, L. D.; Howard, R. E.; Fetter, L. A.; Epworth, R. W.; Tennant, D. M. (1984) *Phys. Rev. Lett.,* **52**, 228-231.
15. Klemic, J. F., Stern, E.; Reed. M. A. (2001) *Nat. Biotechnol.*, **19**, 924-925.
16. Cui, Y.; Wei, Q. Q.; Park, H. K.; Lieber, C. M. (2001) *Science* **293**, 1289-1292.
17. Liess, M. (2002) *Thin Solid Films* **410**, 183-187.
18. Comini, E.; Faglia, G.; Sberveglieri, G.; Pan, Z.; Wang, Z. (2002) *Appl. Phys. Lett.* **81**, 1869-1871.
19. Kong, J.; Franklin, N. A.; Zhou, C. W.; Chapline, M. G.; Peng, S.; Cho, K. J.; Dai, H. J. (2000) *Science* **287**, 622-625.
20. Shimizu, Y. and Egashira M. (1999) *MRS Bull.* **24**, 18-24.
21. Zhang, D.; Li, C.; Han, S.; Liu, X.; Tang, T.; Jin, W. and Zhou, C. *Appl. Phys. A*, **76**, March 2003.
22. R. R. Breaker (2004) Natural and Engineered Nucleic Acids as Tools to Explore Biology. *Nature* 432:838-845.
23. R. R. Breaker (2005) Gene Expression Control: Harnessing RNA Switches. *Gene Ther.* 12:725-726.
24. W. C. Winkler and R. R. Breaker (2005) Regulation of Bacterial Gene Expression by Riboswitches. *Annu. Rev. Microbiol.* 59:487-517.
25. R. Renchovsky and R. R. Breaker. (2005) Computational Design and Experimental Validation of Oligonucleotide-sensing Allosteric Ribozymes. *Nat. Biotechnol.* 23:1424-1433.
26. M. Zivarts, Y. Liu and R. R. Breaker (2005) Engineered Allosteric Ribozymes that Respond to Specific Divalent Metal Ions. *Nucleic Acids Res.* 33:622-631.
27. E Stern, G Cheng, E Cimpoiasu, R Klie, S Guthrie, J Klemic, I Kretzschmar, E Steinlauf, D Turner-Evans, E Broomfield, J Hyland, R Koudelka, T Boone, M Young, A Sanders, R Munden, T Lee, D Routenberg and M A Reed, "Electrical characterization of single GaN nanowires", Nanotechnology 16, 2941 (2005)
28. G. Cheng, E. Stern, D. Turner-Evans, and M. A. Reed, "Electronic properties of InN nanowires", Appl. Phys. Lett. 87, 253101 (2005).
29. E. Stern, G. Cheng, M. P. Young, and M. A. Reed, "Specific Contact Resistivity of Nanowire Devices", Appl. Phys. Lett. 88, 053106 (2006).
30. E. Stern, G. Cheng, C. Li, J. Klemic, E. Broomfield, D. Turner-Evans, C. Zhou, and M.A. Reed, "Methods for Fabricating Ohmic Contacts to Nanowires and Nanotubes", Jour. Vac. Sci. Technol. B24, 231 (2006).

Personnel supported

Breaker lab:
Prof. Ronald Breaker, PI
Dr. Robert Penchovsky (postdoctoral researcher)
Benjamin Boese (graduate student)
Tyler Ames (graduate student)
Lixia Guo (research technician)

Reed lab:
Prof. Mark Reed, PI
Dr. Guosheng Cheng (research scientist)
Dr. Elena Cimpoiasu (postdoctoral researcher)
Ryan Munden (graduate student)
Stan Guthrie (graduate student)

Zhou lab:
Prof. Chongwu Zhou, PI
Chao Li (graduate student)
Fumiaki Ishikawa (graduate student)

Publications

1. "Selective Functionalization of In_2O_3 Nanowire Mat Devices for Biosensing Application", M. Curreli, C. Li, Y. Sun, B. Lei, M. A. Gundersen, M. E. Thompson, and C. Zhou, J. of Am. Chem. Soc. 127, 6922 - 6923 (2005).
2. "Complementary Detection of Prostate Specific Antigen Using In_2O_3 Nanowires and Carbon Nanotubes", C. Li, M. Curreli, H. Lin, F. N. Ishikawa, R. Datta, R. Cote, M. E. Thompson, and C. Zhou, J. of Am. Chem. Soc. 127, 12484 - 12485 (2005).
3. "Complementary Chemical Gating Effect of In_2O_3 Nanowires and Carbon Nanotubes in Response to Low-Density Lipoprotein", T. Tang, X. Liu, C. Li, B. Lei, D. Zhang, M. Rouhanizadeh, T. Hsiai, and C. Zhou, Appl. Phys. Lett. 86, 103903 - 1-3 (2005).
4. "Differentiation of oxidized low density lipoproteins by nanosensors", M. Rouhanizadeh, T. Tang, C. Li, J. Hwang, C. Zhou, T. Hsiai, Sensors and Actuators B, accepted (2005).
5. R. Renchovsky and R. R. Breaker. (2005) Computational Design and Experimental Validation of Oligonucleotide-sensing Allosteric Ribozymes. *Nat. Biotechnol.* 23:1424-1433.
6. M. Zivarts, Y. Liu and R. R. Breaker (2005) Engineered Allosteric Ribozymes that Respond to Specific Divalent Metal Ions. *Nucleic Acids Res.* 33:622-631.
7. E Stern, G Cheng, E Cimpoiasu, R Klie, S Guthrie, J Klemic, I Kretzschmar, E Steinlauf, D Turner-Evans, E Broomfield, J Hyland, R Koudelka, T Boone, M Young, A Sanders, R Munden, T Lee, D Routenberg and M A Reed, "Electrical characterization of single GaN nanowires", Nanotechnology 16, 2941 (2005)
8. G. Cheng, E. Stern, D. Turner-Evans, and M. A. Reed, "Electronic properties of InN nanowires", Appl. Phys. Lett. 87, 253101 (2005).
9. E. Stern, G. Cheng, M. P. Young, and M. A. Reed, "Specific Contact Resistivity of Nanowire Devices", Appl. Phys. Lett. 88, 053106 (2006).
10. E. Stern, G. Cheng, C. Li, J. Klemic, E. Broomfield, D. Turner-Evans, C. Zhou, and M.A. Reed, "Methods for Fabricating Ohmic Contacts to Nanowires and Nanotubes", Jour. Vac. Sci. Technol. B24, 231 (2006).

11. Electropolymerization on Microelectrodes: A Novel Functionalization Technique for Selective Protein and DNA Conjugation, Eric Stern, Steven Jay, James Bertram, Benjamin Boese, Ilona Kretzschmar, Daniel Turner-Evans, Carl Dietz, David A. LaVan, Tadeusz Malinski, Tarek Fahmy & Mark A. Reed, Anal. Chem. in press

Interactions/Transitions

Numerous talk and seminars. No consultations or transitions

New discoveries, patents

Provisional patent filed, "Selective functionalization of microelectrodes"

PTO/SB/16 (12-04)
Approved for use through 07/31/2006. OMB 0651-0032
U.S. Patent and Trademark Office; U.S. DEPARTMENT OF COMMERCE
Under the Paperwork Reduction Act of 1995, no persons are required to respond to a collection of information unless it displays a valid OMB control number.

PROVISIONAL APPLICATION FOR PATENT COVER SHEET

This is a request for filing a PROVISIONAL APPLICATION FOR PATENT under 37 CFR 1.53(c).

Express Mail Label No. EV 750512995 US

INVENTOR(S)		
Given Name (first and middle [if any])	Family Name or Surname	Residence (City and either State or Foreign Country)
Mark	Reed	Monroe, CT
Eric	Stern	New Haven, CT

Additional inventors are being named on the _____ separately numbered sheets attached hereto

TITLE OF THE INVENTION (500 characters max):

Selective Functionalization of Microelectrodes

Direct all correspondence to: **CORRESPONDENCE ADDRESS**

☐ The address corresponding to Customer Number:

OR

☑ Firm or Individual Name: Yale University Office of Cooperative Research

Address: 433 Temple Street

City	State	Zip
New Haven	CT	06511
Country U.S.A.	Telephone 203 436-4675	Fax 203 436-8086

ENCLOSED APPLICATION PARTS *(check all that apply)*

☑ Application Data Sheet. See 37 CFR 1.76
☐ CD(s), Number of CDs _____
☑ Specification *Number of Pages* 15
☒ Other (specify) Figures (pgs. 12-15)
☐ Drawing(s) *Number of Sheets* _____

Application Size Fee: If the specification and drawings exceed 100 sheets of paper, the application size fee due is $250 ($125 for small entity) for each additional 50 sheets or fraction thereof. See 35 U.S.C. 41(a)(1)(G) and 37 CFR 1.16(s).

METHOD OF PAYMENT OF FILING FEES AND APPLICATION SIZE FEE FOR THIS PROVISIONAL APPLICATION FOR PATENT

☑ Applicant claims small entity status. See 37 CFR 1.27.
☐ A check or money order is enclosed to cover the filing fee and application size fee (if applicable).
☐ Payment by credit card. Form PTO-2038 is attached
☑ The Director is hereby authorized to charge the filing fee and application size fee (if applicable) or credit any overpayment to Deposit Account Number: 250110. A duplicative copy of this form is enclosed for fee processing.

TOTAL FEE AMOUNT ($): 100.00

The invention was made by an agency of the United States Government or under a contract with an agency of the United States Government.
☐ No.
☑ Yes, the name of the U.S. Government agency and the Government contract number are: ARO (DAAD19-01-1-0592), AFOSR (F49620-01-1-0358), NASA (NCC 2-1363)

SIGNATURE James G. Boyle Date 12/2/05

TYPED or PRINTED NAME James G. Boyle REGISTRATION NO. _____ *(if appropriate)*

TELEPHONE 203-436-8092 Docket Number: 4205

USE ONLY FOR FILING A PROVISIONAL APPLICATION FOR PATENT

This collection of information is required by 37 CFR 1.51. The information is required to obtain or retain a benefit by the public which is to file (and by the USPTO to process) an application. Confidentiality is governed by 35 U.S.C. 122 and 37 CFR 1.11 and 1.14. This collection is estimated to take 8 hours to complete, including gathering, preparing, and submitting the completed application form to the USPTO. Time will vary depending upon the individual case. Any comments on the amount of time you require to complete this form and/or suggestions for reducing this burden, should be sent to the Chief Information Officer, U.S. Patent and Trademark Office, U.S. Department of Commerce, P.O. Box 1450, Alexandria, VA 22313-1450. DO NOT SEND FEES OR COMPLETED FORMS TO THIS ADDRESS. **SEND TO: Commissioner for Patents, P.O. Box 1450, Alexandria, VA 22313-1450.**

If you need assistance in completing the form, call 1-800-PTO-9199 and select option 2.

Honors/awards: none

Representative publications, follow

nature biotechnology

Computational design and experimental validation of oligonucleotide-sensing allosteric ribozymes

Robert Penchovsky & Ronald R Breaker

Allosteric RNAs operate as molecular switches that alter folding and function in response to ligand binding. A common type of natural allosteric RNAs is the riboswitch; designer RNAs with similar properties can be created by RNA engineering. We describe a computational approach for designing allosteric ribozymes triggered by binding oligonucleotides. Four universal types of RNA switches possessing AND, OR, YES and NOT Boolean logic functions were created in modular form, which allows ligand specificity to be changed without altering the catalytic core of the ribozyme. All computationally designed allosteric ribozymes were synthesized and experimentally tested *in vitro*. Engineered ribozymes exhibit >1,000-fold activation, demonstrate precise ligand specificity and function in molecular circuits in which the self-cleavage product of one RNA triggers the action of a second. This engineering approach provides a rapid and inexpensive way to create allosteric RNAs for constructing complex molecular circuits, nucleic acid detection systems and gene control elements.

The detection of specific chemical and biological compounds can be achieved with structured RNAs that form selective binding pockets for their target ligands[1]. These ligand-binding domains, or aptamers[2,3], can be used independently[4–6] or can be joined with other functional RNA domains[7–9] to serve as molecular reporter systems that selectively bind targets and signal their presence to the user. For example, aptamers have been judiciously coupled to catalytic RNA domains to form allosteric ribozymes whose activities in many cases are modulated by several orders of magnitude upon ligand (or 'effector') binding[8].

The potential utility of allosteric ribozymes has been demonstrated by the construction of prototype RNA sensor arrays that have been used to detect specific proteins, small molecules and metal ions that are present even in complex biological mixtures[10,11]. Furthermore, it has recently been discovered that numerous natural RNA switches, or riboswitches, exist in many bacteria[12–15] and in some higher organisms[16,17], where they serve as metabolite-sensing gene control elements[18–20]. The fact that modern organisms rely on riboswitches supports the hypothesis that nucleic acids provide a robust medium for the construction of such functional macromolecules. Indeed, novel allosteric RNAs might be engineered for a broad range of practical applications[1] in areas such as gene therapy[21,22], designer gene control systems[23–27], biosensors[10,11,28–30] and molecular computation[31,32].

The fusion of aptamers with ribozymes to create RNA switches most commonly has been achieved by modular rational design[33,34], or by blending modular rational design with *in vitro* evolution techniques[35–37]. Modular rational design approaches are most effective for designing oligonucleotide-responsive ribozymes[38–41] or deoxyribozymes[42,43], largely because the rules that govern molecular recognition and structural characteristics of Watson-Crick base-paired interactions are well understood. However, it remains problematic to design allosteric nucleic acids that exhibit robust activation, that are triggered without introducing denaturation and reannealing steps and that process to near completion.

In this study, we describe a computational strategy for designing new allosteric ribozyme constructs that exhibit robust allosteric activation upon the addition of specific oligonucleotides. A partition function algorithm[44] was used to design RNAs that are predicted to form a dominant secondary structure in the absence of an oligonucleotide effector. This folded pattern is predicted to be distinct from the secondary structure that dominates in the presence of a matched oligonucleotide effector. The algorithm computes the entire ensemble of possible secondary structures as a function of temperature[45], which allows the user to choose to build only those constructs that are predicted to exhibit the desired molecular switch characteristics.

This automated design method can be used to generate a large number of allosteric ribozymes with predefined properties within hours by assessing millions of different sequences on a personal computer. We demonstrate the utility of this method by designing and testing four universal types of molecular switches possessing AND, OR, NOT and YES Boolean logic functions. Each ribozyme construct has a modular architecture, which allows an oligonucleotide binding site (from 16 to 22 nt in length) to be computationally altered, thus maintaining specific and uniform allosteric function.

RESULTS

Architecture and design of allosteric hammerhead ribozymes

As is observed with allosteric proteins, RNAs with allosteric function undergo alternative folding of their polymeric structure upon effector binding, which modulates of function at a site that is distal from

Department of Molecular, Cellular and Developmental Biology, Yale University, PO Box 208103, New Haven, Connecticut 06520-8103, USA. Correspondence should be addressed to R.R.B. (ronald.breaker@yale.edu).

Received 12 April; accepted 4 September; published online 23 October 2005; doi:10.1038/nbt1155

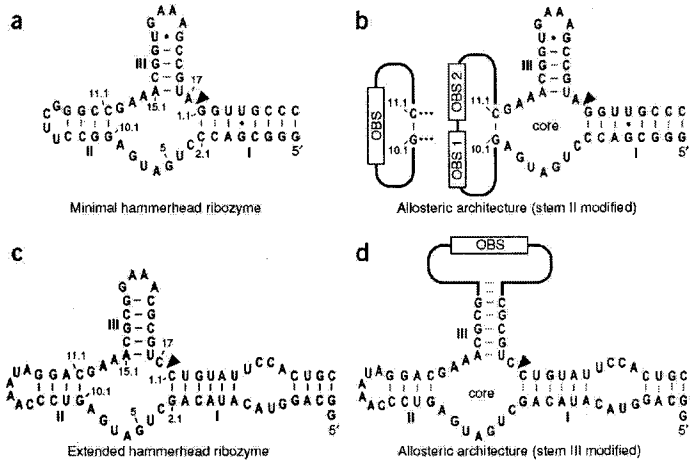

Figure 1 Design architectures for the construction of oligonucleotide-responsive hammerhead ribozymes. (**a**) Parental hammerhead ribozyme sequence used previously[33–36] and in the current study to create ligand-responsive ribozyme switches. Numbering systems for the hammerhead is as described elsewhere[52], where stems I through III represent base-paired structures that are essential for ribozyme function. The arrowhead identifies the site of ribozyme self-cleavage. (**b**) Integration of one (left) or two (right) oligonucleotide binding sites (OBS) into stem II of the parent hammerhead depicted in **a**. (**c**) Extended hammerhead ribozyme that exhibits faster RNA cleavage rates with low Mg^{2+} concentrations[53]. (**d**) Integration of an OBS in stem I of the extended ribozyme to create RNA switches with NOT function.

where the effector has bound. In the case of RNA, stable secondary structures can fold on a time scale of microseconds, and these core elements typically control the subsequent formation of tertiary contacts[46–48]. The energies involved in secondary structure formation typically are much greater than those of tertiary contacts[49]. Thus, a substantial amount of the folding energy that establishes RNA conformations can be modeled at the secondary structure level[50]. However, alternative stable conformations could form at various stages of the folding process and trap the molecule into an inactive conformation. Thus, a broader landscape of folding potential should be taken into account to minimize the probability of encountering such misfolded conformers.

The precise secondary structure required for the hammerhead ribozyme to promote RNA transesterification is well known (**Fig. 1a**)[51,52]. Variations in sequence composition that preclude formation of this essential secondary structure most likely will result in reduced activity, or no activity at all. Allosteric ribozymes can exploit this character of RNA structure by harnessing binding energy involved in effector-RNA complex formation to shift folding patterns or pathways to favor either active or inactive states. If these states are separated by a large energy barrier (e.g., strong base-pairing interactions must be disrupted to exchange states), then the ribozyme cannot transition easily between the two states without more proactive denaturation and reannealing. In contrast, if the energy barrier between the two states is small, then the ribozyme might exhibit a poor dynamic range for modulation by the effector. It is these aspects of allosteric ribozyme design that have been most difficult to anticipate and control during the design process.

The architecture of most ribozyme constructs chosen for this study exploit the sequence versatility of nucleotides residing in stem II of the hammerhead ribozyme (**Fig. 1b**). This same region has been used extensively as the location for grafting aptamers when creating numerous other allosteric ribozyme constructs[10,33–36]. An extended hammerhead construct (**Fig. 1c**) was used to introduce allosteric binding sites into stem III (**Fig. 1d**). A two-step computational procedure was applied to design allosteric hammerhead ribozymes that modulate their cleavage activity only in the presence of predefined oligonucleotides. In the first step, a large number of random sequences ($\geq 10^7$) residing within the effector binding site(s) were examined computationally using a random search algorithm based on the partition function for formation of dominant secondary structures[44] in the presence and absence of effector molecules with different lengths. Nucleotide sequences residing within an oligonucleotide binding site (OBS) must satisfy two criteria for a given construct to be chosen for testing. First, OBS nucleotides must be predicted to participate in forming stable but inactive secondary structure (OFF state) in the absence of an effector oligonucleotide. Second, OBS nucleotides must stably pair with the effector DNA and liberate adjoining nucleotides that are predicted to form a stable stem II structure that allows activation of the ribozyme domain (ON state).

Design and characterization of ribozymes with YES function

Using the approach described above, we generated a series of five RNA constructs that were predicted to function as RNA switches with molecular YES logic. Molecules with attributes of YES logic function must remain inactive unless receiving a single molecular impulse that triggers activity. One of these constructs, termed YES-1, is predicted to form the desired OFF- and ON-state structures in the absence and presence, respectively, of a 22-nt effector DNA (DNA-1; **Fig. 2a**). In its inactive conformation, the nucleotides within the OBS are proposed to form a stem IV structure. Stem IV involves extensive base-pairing interactions with portions of the hammerhead core and with most nucleotides that would otherwise form the stem II structure required for ribozyme activation. In the presence of DNA-1, a major portion of the nucleotides in stem IV would become sequestered by intermolecular base pairing, and nucleotides that can participate in stem II formation are liberated.

The results of the computational assessment of the structure-forming potential of this construct are visually represented by dot matrix plots (**Fig. 2a**, right). It is apparent from these plots that the probability of forming stem IV or several base-pairing alternatives is high, whereas there is no indication that stem II has any reasonable chance of forming. In contrast, repeating the computation in the presence of the DNA effector drastically reduces the probability that stem IV can form and thus increases the probability that stem II will be formed. It is notable that the probabilities for forming hammerhead stems I and III remain largely unaffected by the

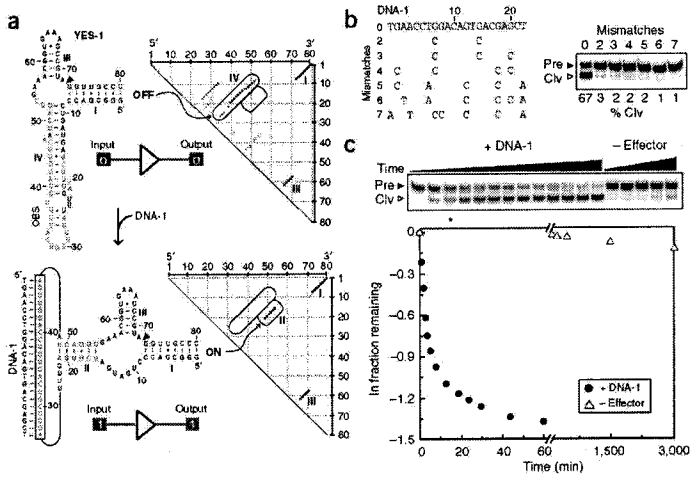

Figure 2 Design and characterization of an oligonucleotide-specific RNA switch possessing YES logic function. (**a**) Secondary structure models for the most stable conformers as computed using the partition function algorithm in the absence (OFF) or presence (ON) of a 22-nucleotide DNA effector. The effector-binding site (light blue) is joined to nucleotides 10.1 and 11.1 of the hammerhead core via eight- and six-nucleotide linkers. In the ON state, most of these linker nucleotides are predicted to form an extended stem II structure (red). To the right of each model is a dot matrix plot wherein larger points reflect greater probability of base pairing. Encircled points reflect the main differences in predicted structures between the OFF (stem IV) and ON (stem II) states. Nucleotides 1 through 79 are numbered from 5′ to 3′ across the top and right of the plots. Schematic representations of the logic states of the constructs are shown in this and subsequent figures. (**b**) Selective activation of ribozyme self-cleavage by an effector DNA complementary to the OBS. Radiolabeled ribozymes (5′ ^{32}P, Pre) undergo self-cleavage only with the perfectly matched DNA effector (0 mismatches) and the resulting radiolabeled cleavage fragment (Clv) is separated from the precursor by denaturing 10% PAGE. Products were visualized and cleavage yields were quantified by PhosphorImager. (**c**) Kinetics of ribozyme (1 μM) self-cleavage in the presence (+) of perfectly matched 22-nt effector DNA (3 μM) and in the absence (–) of effector DNA. Gel image is as described in **b**. Plot using data derived from the gel depicts the natural logarithm of the fraction of RNA remaining uncleaved versus time.

presence or absence of the effector DNA. In a subsequent stage of the design procedure, the secondary structure adopted for the YES-1 ribozyme was used as a basis to compute the folding properties of additional allosteric ribozyme candidates that are likely to have very similar RNA energy folding landscapes but that carry different OBS sequences that respond to different effector DNAs.

Five sequences obtained from this computational design process, representing extreme cases in terms of the selection thermodynamics criteria used during computation, were arbitrarily chosen for synthesis and testing. Each RNA construct was prepared by transcription *in vitro* using radiolabeled nucleotides. The YES-1 RNA construct (**Fig. 2a**) is representative of ribozyme constructs that were computed to be thermodynamically less stable in their inactive states (free energy based on the partition function at 37 °C, $E_p = -35.6$ kcal mol^{-1}) and are predicted to have the potential to form several alternative secondary structures that all preclude formation of stem II.

The performance characteristics of the first RNA, YES-1, was tested by incubation of internally ^{32}P-labeled RNAs with a matched effector DNA of 22 nt, or with a series of mutant DNAs that carry two through seven mismatches relative to the matched effector DNA (**Fig. 2b**). Robust self-cleavage was observed only when the perfectly matched effector DNA was present, whereas as few as two mismatches caused complete loss of activation under these assay conditions. From these data, we conclude that the thermodynamic stability of the OFF state for YES-1 is sufficiently greater than that of the ON state in the absence of effector DNA ($E_p = -29$ kcal mol^{-1}, difference = 6.6 kcal mol^{-1}) such that the vast majority of the RNA constructs reside in the inactive conformation during assay incubation.

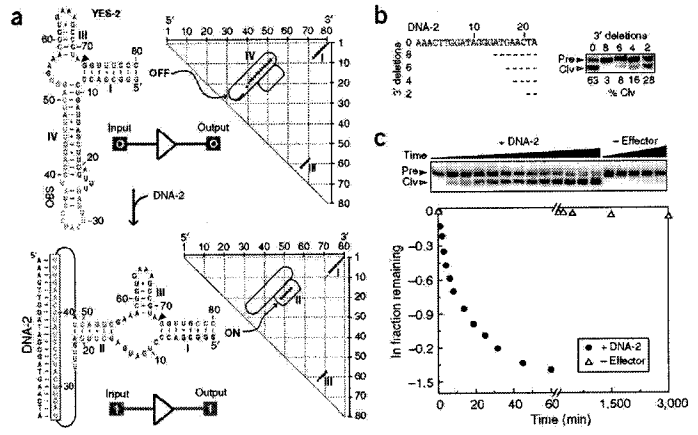

Figure 3 Design and characterization of YES-2, a variant of YES-1 that exhibits altered oligonucleotide specificity. (**a**) Secondary structure models for the most stable conformers in the absence (OFF) or presence (ON) of a 22-nucleotide DNA effector complementary to the changed OBS. (**b**) Selective activation of YES-2 self-cleavage by effector DNAs complementary to the OBS. (**c**) Kinetics of YES-2 self-cleavage in the presence of perfectly matched 22-nt effector DNA and in the absence of effector DNA. For additional details, see the legend to **Figure 2**.

To estimate the dynamic range for allosteric activation, or the total range of rate constant enhancement brought about by effector binding, we conducted a time course for ribozyme self-cleavage in the presence and absence of the matched effector DNA (**Fig. 2c**). In the presence of the effector, the apparent rate constant observed for ribozyme activity (apparent k_{obs}) is $\sim 1.1 \times 10^{-1}$ min^{-1}, whereas the apparent k_{obs} for the ribozyme in the absence of effector DNA is $\sim 1.6 \times 10^{-5}$ min^{-1}. These results indicate that the allosteric dynamic range is nearly 7,000-fold, and the maximum rate constant is within tenfold of the typical maximum activity for the unmodified hammerhead ribozyme core (~ 1 min^{-1}) measured under similar conditions[33]. Furthermore, the stability of the OFF-state structure is not so extreme or so rapidly adopted that activation by the effector DNA is precluded when reaction buffer (**Fig. 2b**) and DNA are introduced simultaneously to the YES-1 ribozyme.

Approximately 21% of the YES-1 RNAs that are incubated for 60 min in the presence of effector DNA remain uncleaved, suggesting that perhaps defects in RNA integrity or alternately folded RNAs preclude proper function of all RNAs in the reaction. To confirm the apparent k_{obs} value reported for ribozyme-effector complexes, we conducted additional experiments using 6 μM of effector DNA. The curve obtained was completely overlapping with that obtained when 3 μM effector DNA was used (data not shown), indicating that the ribozymes were saturated with effector DNA.

Similarly, the performance characteristics of a second ribozyme, YES-2 (**Fig. 3**), were established. YES-2 was selected for testing because it is predicted to be more stable in its OFF state ($E_p = -39$ kcal mol^{-1}) than YES-1, although it has a greater difference between the OFF- and ON-states ($E_p = -29$ kcal mol^{-1}, difference = 10 kcal mol^{-1}). This increase in predicted stability for stem IV yields dot matrix plots that suggest only one OFF-state structure that has a high probability of forming (**Fig. 3a**), whereas the addition of the effector DNA (DNA-2) that matches the new OBS sequences yields a predicted structure for the ribozyme domain that is identical to that for YES-1.

For this series of experiments, we tested the specificity of effector-mediated activation by using DNAs that differ from the matched YES-1 effector DNA by truncation **Fig. 3b**). Although the shortest effector DNA exhibits almost no activation of the YES-2 ribozyme, longer DNAs induce progressively greater yields, with the full-length effector DNA promoting ribozyme cleavage with a yield that is similar to that generated by the YES-1 ribozyme under identical reaction conditions (**Fig. 2b**).

The apparent k_{obs} values exhibited by the YES-2 ribozyme in the presence and absence of its matched 22-nt effector DNA also were similar to those observed for YES-1 (**Fig. 3c**), despite the differences in thermodynamic stability and predicted structural heterogeneity between the two constructs. Specifically, the dynamic range for YES-2 is $\sim 8{,}000$ with apparent k_{obs} values of 1.2×10^{-5} min^{-1} and 0.1 min^{-1} in the absence and presence of DNA-2, respectively.

Approximately 25% of YES-2 RNAs remain uncleaved after a 60-min incubation with the full-length DNA-2 (**Fig. 3c**), again suggesting that chemical integrity and/or folding uniformity are not absolute.

Similar molecular switch functions were obtained for the remaining three related constructs (YES-3, YES-4 and YES-5; **Supplementary Figs. 1–3** online), demonstrating that new RNA switches that respond to distinct DNA effectors can be designed routinely. Furthermore, these constructs function as 'rapid switches,' wherein the addition of the matched effector DNA induces activity in an RNA that had been folded into its inactive structure (**Supplementary Figs. 1–3** online). Alternatively, a construct that was intentionally designed to form an exceptionally stable OFF state structure (YES-6) remains inactive as expected, even upon the introduction of its matched DNA effector (**Supplementary Fig. 4** online). These results indicate that the computational method used to design multistate oligonucleotide-responsive ribozyme structures is robust and has a high probability of accurately predicting allosteric function. With the 22-nt long allosteric binding sites, there are 1.76×10^{13} possible sequence combinations, thus providing an enormous diversity of possible effector specificities. We predict that at least 5% of all possible combinations, or nearly a trillion different sequence combinations of 22-nt DNAs, will meet the rigorous criteria used in this study when designing candidate YES gates.

Design and characterization of a ribozyme with NOT function

An extended natural hammerhead ribozyme (**Fig. 1c**) from *Schistosoma mansoni* was used as the parent construct for the design of a ribozyme that is deactivated by allosteric interactions with oligonucleotides. This ribozyme exhibits faster RNA cleavage kinetics and requires lower concentrations of Mg^{2+} to trigger activity[53]. Allosteric constructs derived from parental ribozymes with these properties are more likely to function *in vivo* where divalent ion concentrations are low and where fast ribozymes might be needed.

Extended hammerhead ribozymes exhibit improved function because they form a tertiary structure between the loop sequences of stem II and a bulge within stem I[54–56]. Therefore, the OBS was relocated to stem III to design a construct that functions as a NOT gate (**Fig. 1d**) so these critical ribozyme tertiary-structure contacts would not be disrupted. The resulting design, termed NOT-1 (**Fig. 4a**) is predicted to form (**Supplementary Fig. 5** online) a single major ON state structure ($E_p = -30.55$ kcal mol^{-1}) in the absence of effector DNA-6 (23 nt), and is predicted to form a single major structure in its effector-bound OFF state that has an extended stem I and a disrupted stem III ($E_p = -25.46$ kcal mol^{-1}).

If the NOT-1 construct functions as predicted and self-cleaves in the absence of effector DNA, preparation of the RNA is expected to pose a

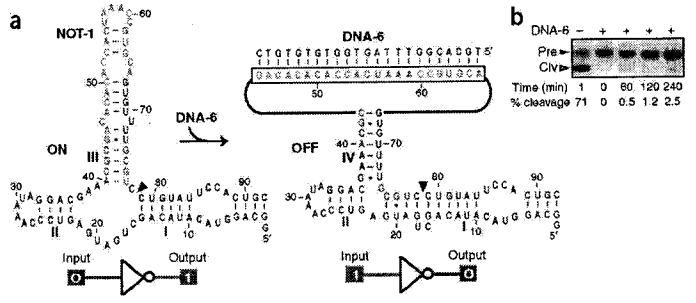

Figure 4 Design and characterization of NOT-1 based on an extended hammerhead ribozyme. (**a**) Secondary structure models for the most stable conformers predicted in the absence (ON) and presence (OFF) of a 23-nucleotide effector. Dot matrix plots for the construct are presented in **Supplementary Figure 5** online. (**b**) Deactivation of NOT-1 by a DNA complementary to the OBS.

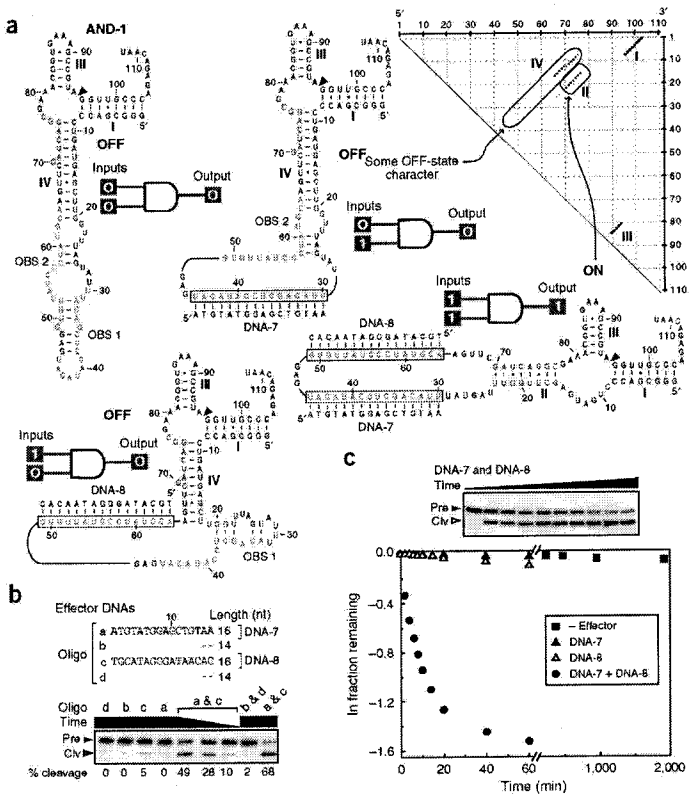

Figure 5 Design and characterization of AND-1, an oligonucleotide-specific molecular switch that possesses AND logic function. **(a)** AND-1 is designed to form the active hammerhead structure and self-cleave only when presented simultaneously with its two corresponding effector DNAs (DNA-7 and DNA-8). The dot matrix plots for the ON state showing some character of the OFF states (stem IV) is depicted. Dot matrix plots for the three OFF states are presented in **Supplementary Figure 7** online. **(b)** Activation of AND-1 self-cleavage requires both full-length DNA-7 and DNA-8 effectors. Maximum incubation time is 60 min. **(c)** Kinetics of AND-1 self-cleavage under various combinations of effector DNAs. Details are as described in the legend to **Figure 2**.

problem because the ribozyme could self-cleave during transcription *in vitro*. To avoid this, we carried out transcription of NOT-1 DNA templates in the presence of 10 μM DNA-6 and 10 μM of the antisense oligonucleotide CTCATCAGC. The latter DNA is complementary to nucleotides 15 through 23 of the NOT-1 hammerhead core. Although the NOT-1 RNA exhibited only ~25% self-cleavage when produced by transcription under these conditions (data not shown), the RNA exhibited robust self-cleavage activity ($k_{obs} > 1$ min^{-1}) when incubated in the absence of DNA-6 (**Fig. 4b**). Similarly, addition of excess effector oligonucleotide to a NOT-1 ribozyme assay caused strong inhibition.

Design and characterization of a ribozyme with AND function

Molecules with attributes of AND logic function must remain inactive unless receiving two separate molecular impulses that trigger activity. Candidate RNA constructs possessing AND logic function triggered by 16-nt effector DNAs were designed using the same principles and computational procedures used to identify candidate YES RNA switches. However, additional steps were added to permit computation of four different structural states with high stability. As with the YES gate computations, one of the structural states must permit formation of the active hammerhead core, in this case, only when presented with two effector DNA sequences. The remaining three states should not permit ribozyme function even if either of the two effector DNAs are present independently. Our computational search efforts indicated that many thousands of ribozymes with the same AND gate properties can be generated.

We chose to test the function of one computationally designed AND gate candidate termed AND-1. The most probable secondary structure models for all four states of AND-1 and dot matrix plots for the predicted ON state are depicted in **Fig. 5a**. This RNA construct is predicted to have a thermodynamic stability in the absence of effector DNAs (E_p = −46.97 kcal mol^{-1}) that is ~15 kcal mol^{-1} more stable than the structure representing the active ribozyme state (E_p = −31.9 kcal mol^{-1}). The predicted stabilities of the RNA structures are intermediate when either effector DNA-7 (E_p = −39.50 kcal mol^{-1}) or effector DNA-8 (E_p = −36.30 kcal mol^{-1}) are bound independently. It is notable that, in the presence of both effectors, AND-1 is predicted to have approximately equal possibility for formation of stem II and a portion of stem IV, despite the docking of both effector DNAs (**Fig. 5a** and **Supplementary Fig. 6** online).

The general structural characteristics of AND-1 permit the ribozyme to remain largely inactive in the absence of effector DNAs, or in the presence of either DNA-7 or DNA-8 (**Fig. 5b**). However, the addition of both effector DNAs triggers robust ribozyme activity. The AND-1 ribozyme also is sensitive to the length of the effector DNAs. Although both 16-nt effector DNAs are needed to trigger AND-1 function, truncation of either DNA by deletion of two nucleotides at their 3′ terminus renders the system inactive, regardless of what combination of full-length and truncated DNAs are used (**Fig. 5b**).

To confirm our observations, we experimentally established rate constants for all four states with 1 μM AND-1 ribozyme incubated under standard reaction conditions (**Fig. 2b** legend) without and with 3 μM effector DNAs (**Fig. 5c**). Again, as computationally predicted, the AND-1 ribozyme exhibited very low self-cleavage activity in the absence of effector DNAs (apparent k_{obs} = 2.4 × 10^{-5} min^{-1}), and these poor apparent k_{obs} values persisted when either effector DNA-7 (1 × 10^{-4} min^{-1}) or effector DNA-8 (9 × 10^{-4} min^{-1}) were added independently. In contrast, the addition of both effectors induced an ~5,000-fold increase in the apparent k_{obs} value (0.11 min^{-1}) relative

to that exhibited by AND-1 in the absence of effector DNAs. This maximum apparent k_{obs} value increases to 0.5 min^{-1} when a single U-to-C change is made at nucleotide 18 (**Fig. 5a**), which strengthens base pairing in stem II (data not shown). Given the robust activity of the AND-1 ribozyme and its variant when activated, and given the extent to which these RNAs proceed towards complete processing, it is likely that the stem II structure dominates over the stem IV element (**Fig. 5a**) when presented with both effector DNAs, or at least the two stems are in rapid equilibrium.

Design and characterization of a ribozyme with OR function

The design of allosteric hammerhead ribozymes possessing OR logic function was conducted in a similar manner to that used to computationally identify AND gate candidates. Again four different states were computed, but in this case we sought to create three ON-state structures and only one OFF-state structure. Again, our computational search results indicate that many thousands of ribozymes with OR logic function can be designed. One candidate construct chosen for biochemical analysis, termed OR-1 (**Fig. 6a** and **Supplementary Fig. 7** online), carries only three nucleotide changes relative to the AND-1 RNA construct depicted in **Fig. 5a**. As with the other RNA logic gates described above, the most probable OFF state for OR-1 is thermodynamically more stable (E_p = –46.5 kcal mol^{-1}) than any of the ON-state structures that permit the formation of stem II (E_p = –33.9 kcal mol^{-1} when both effectors are bound).

The function of OR-1 also was tested for oligonucleotide-induced ribozyme activity. As predicted, OR-1 undergoes little self-cleavage in the absence of effector DNAs, but exhibits robust activity when presented with any combination of effectors DNA-9 and DNA-10, which are 22-mer oligonucleotides that are complementary to OBS sites 1 and 2, respectively (**Fig. 6b**). Similarly, the allosteric dynamic range for OR-1 was estimated by examining the kinetics of ribozyme cleavage (**Fig. 6c**) in the absence of effector DNA (apparent k_{obs} = 2.3 × 10^{-4} min^{-1}) and in the presence of both DNA-9 and DNA-10 (apparent k_{obs} = 0.9 min^{-1}). The dynamic range of this ribozyme is ~4,000-fold under standard assay conditions. In an assay mixture that more closely approximates physiological conditions (50 mM Tris-HCl, pH 7.5 at 23 °C, 100 mM KCl, 25 mM NaCl, and 2 mM $MgCl_2$) the k_{obs} was found to be about 0.3 min^{-1} at 37 °C (data not shown). Similar to that observed with AND-1, the k_{obs} value for the OR-1 construct improved to 0.5 min^{-1} under these assay conditions when position 18 was mutated to a C residue (data not shown). Moreover, three additional constructs with OR logic function that respond to the same effector DNAs were created, which exhibited properties similar to those of OR-1 (**Supplementary Fig. 8** online).

Molecular circuit based on RNA switches with YES function

A possible attractive feature of molecular logic gates is the ability to generate signals that can control the activity of other molecular switches. The production of a diversity of oligonucleotide-sensing ribozymes would expand the complexity and efficiency of engineered nucleic acid circuits like those demonstrated previously[31,32].

To demonstrate inter-ribozyme communication, we used construct YES-1 and a variation of construct YES-2 to create a simple molecular circuit (**Fig. 7a**). The sequence and length of YES-2 was altered in stem I to create a YES-2 variant that generates a new 21-nt 3′ fragment upon self-cleavage (**Fig. 7a**). This RNA fragment is complementary to the OBS of YES-1, and therefore it should activate the second ribozyme upon cleavage and dissociation from the first ribozyme in the circuit.

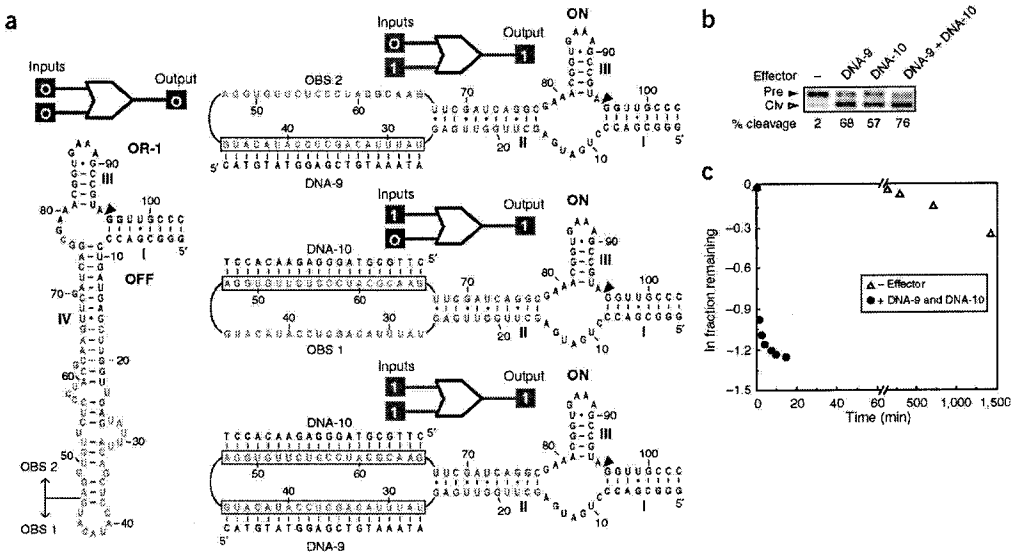

Figure 6 Design and characterization of OR-1, an oligonucleotide-specific molecular switch that possesses OR logic function. (**a**) OR-1 is designed to trigger self-cleavage when either effector (DNA-9 or DNA-10) or both effectors are present. Dot matrix plots for each of the four structures are presented in **Supplementary Figure 7** online. (**b**) Activation of OR-1 self-cleavage occurs when either or both effectors are present when incubated for 5 min under standard assay conditions. (**c**) Kinetics of OR-1 self-cleavage in the absence of effector and in the presence of both effector DNAs. Details are as described in the legend to **Figure 2**.

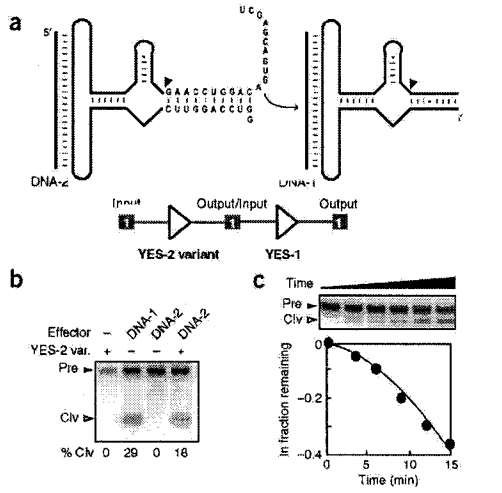

Figure 7 A two-step ribozyme signaling pathway constructed using YES-1 and a variant of YES-2. (**a**) Nucleotides of the YES-2 variant RNA that differ from YES-2 are depicted. Upon activation of YES-2 variant by effector DNA-2, the 3′ cleavage fragment (RNA-1) is released and serves as an effector for YES-1 activation. (**b**) Assay depicting function of a ribozyme-signaling pathway. YES-1 RNAs are radiolabeled in all lanes. Ribozymes and effector DNAs are present as defined at concentrations of 1 and 3 μM, respectively, and reactions were incubated at 23 °C for 5 min. Other details are as described for **Figure 2**. (**c**) Kinetic analysis of YES-1 self-cleavage in the presence of YES-2 variant and its effector DNA-2. Details are as described in **b**.

This simple molecular signaling pathway was demonstrated using radiolabeled YES-1 with various combinations of unlabeled YES-2 and the oligonucleotides DNA-1 and DNA-2. Although DNA-1 triggers YES-1 cleavage as demonstrated previously (**Fig. 2**), no cleavage is observed when both ribozymes are simultaneously incubated in the absence of DNA effector (**Fig. 7b**). This demonstrates that the YES-1 ribozyme is not activated when its RNA-1 signal oligonucleotide remains attached to the YES-2 variant ribozyme. In contrast, the addition of DNA-2 induces YES-1 cleavage only when the YES-2 variant ribozyme is present. Furthermore, the kinetics of YES-1 function as part of the complete signaling pathway are indicative of a lag phase that we interpret to be caused by the time required to release RNA-1 from the YES-2 variant upon activation by DNA-2 (**Fig. 7c**).

These findings are consistent with the design of a ribozyme-signaling pathway in which an activator of the first ribozyme in the series triggers release of an activator of the second ribozyme. Although this circuit is simple in design, our findings suggest that one could construct more complex molecular circuitries in which oligonucleotide triggers carry out various logic-based ribozyme functions.

DISCUSSION

In this study, we have used a computational approach to design various oligonucleotide-responsive ribozymes. Of 11 designs constructed based on the general architectures depicted in **Figure 1**, all of them functioned as robust RNA switches that exhibit at least three orders of magnitude in rate enhancement and large rate constants for cleavage once activated. This high probability of choosing functional designs is possible because the principles of RNA secondary-structure folding largely follow the simple rules of Watson-Crick base pairing, and the thermodynamic parameters for base-pair interactions are available.

One important advantage of the designs generated by this computational approach is that elements of the constructs can be treated as tunable modules, which makes possible the generation of large numbers of ribozymes with tailored functions by making only a few rational changes. This modularity can be exploited to more rapidly produce variant RNA switches that exhibit distinct effector specificities compared with *in vitro* selection, which might have to be repeated for each new target oligonucleotide. Even more sophisticated RNA switches that further mimic the properties of natural riboswitches (e.g., cooperative ligand binding[57]) or that exhibit more complex sensory and control functions might be computationally engineered. However, precise control over the folding and function of the RNA constructs must be retained or the designs will result in progressive erosion of ribozyme activity as more features are added.

The application of a partition function algorithm for computing base-pairing probabilities[44] allows RNA engineers to estimate the likelihood that certain secondary structure elements will form preferentially over others, and the computing power of desktop systems permits one to survey the full RNA energy landscape for millions of possible sequences with a reasonable expenditure of time. With only a few days of computational time, the scale of the different effector and ribozyme sequences explored could match the initial pool size sometimes used for *in vitro* selection experiments ($\sim 10^{15}$ molecules). Running several computational processes simultaneously would further reduce the computational time needed for these analyses to only a few hours.

Although the design process used here accounts for the thermodynamic stability of various base-paired structures in the absence or presence of effector oligonucleotides, it does not autonomously examine all aspects that determine the compatibility of structures formed by effector binding and structures required for catalysis. For example, the linkers between the OBS and stem II of the ribozyme for both YES-1 (**Fig. 2a**) and YES-2 (**Fig. 3a**) appear to constrain the distance between the end of an OBS-effector helix and one end of stem II of the ribozyme. This distance-constraint problem becomes even more evident in the designs of NOT-1 and OR-1. For example, the OR-1 secondary structure model as depicted (**Fig. 6a**) would require a 180° turn of the RNA backbone to accommodate two rigidly formed OBS-effector interactions. Since this structure might be substantially strained, the RNAs might carry localized variations compared with the secondary structure models depicted. Whether all the base pairs involved in these two interactions can form simultaneously as modeled, or whether some base pairs must be denatured or otherwise distorted to approximate this secondary structure model is not considered by our current algorithm. Although these possible requirements for structural distortion do not prevent the computational design approach from providing functional RNA switches, future design efforts undoubtedly would be improved by taking into account these higher-ordered conformational features.

Most engineered ribozymes described in this study are based on a minimized version of the hammerhead ribozyme that typically exhibits a rate constant for RNA cleavage of no greater than 1 min^{-1}. Therefore, engineered oligonucleotide-responsive ribozymes based on this catalytic RNA are limited in their speed and possible

utility. For example, the most active ribozymes designed in this study might not be sufficiently fast to influence the expression of genes in bacteria, which exhibit lifetimes that are typically measured in seconds or minutes. However, slightly larger variants of this ribozyme core[53–56] catalyze RNA cleavage with rate constants that are as large as 10^4 min^{-1}. Therefore, engineered constructs based on these enhanced self-cleaving ribozymes, such as NOT-1 (**Fig. 4**), could serve as high-speed oligonucleotide-responsive switches for building more complicated computational circuits[31,32] and biosensor devices[1]. High-speed RNA switches also could be used as components of designer genetic circuits[25,58–60]. Multiple different oligonucleotide-sensing ribozymes could be embedded within different reporter gene constructs with overall architectures that enable sensing the expression of mRNAs, noncoding nucleic acids or externally delivered oligonucleotide effectors.

METHODS

Design of RNA switches possessing different logic functions. The design of oligonucleotide-specific allosteric ribozymes was performed in two stages by adapting an existing random search algorithm for generating DNA libraries for molecular computing[61]. In stage 1, four different types of hammerhead ribozymes representing AND, OR, YES and NOT Boolean logic functions were selected by computing RNA secondary structures based on the equilibrium partition function as described by McCaskill[44]. Our use of this approach relies on the application of thermodynamic parameters using essentially the RNAfold source code from the Vienna RNA folding package[62–64].

For three switch types (AND, OR and YES), constructs were designed such that the nucleotides forming stem II of the hammerhead were held constant, whereas the adjoining loop sequences were randomized. The search algorithm selects for variations of loop sequences that permit portions of the stem II pairing elements to form alternative structure in the absence of effector DNAs. The design of the NOT construct was conducted using the same search algorithm, but the loop sequences adjoining stem III were varied. To simulate the presence of the effector DNA the nucleotides within the OBS elements are defined as having no potential to form secondary structure with the remainder of the construct. Two different states representing the absence and presence of DNA effector were computed for YES and NOT gates. Four different states were computed for OR and AND gates.

In stage 2, the different types of RNA switches were used as matrices for generating sets of ribozyme constructs that have OBS elements with distinct sequences. For example, the random search algorithm applied for the design of YES gates for stage 1 (1.X) and stage 2 (2.X) is outlined below. See also a flow chart for this computational procedure depicted in **Supplementary Figure 9** online.

1.1. Generate a new random OBS, from 16 to 22 nt long, over the alphabet of A, U, C, G. The sequences should not have four or more consecutive identical nucleotides.

1.2. Insert the OBS into the predefined RNA sequence GGGCGACCCU GAUGAGCUUGAGUUU$(X)_{16-22}$AUCAGGCGAAACGGUGAAAGCCGUAGG UUGCCC that contains the hammerhead motif.

1.3. Fold the sequence obtained and calculate the free energy at 37 °C of the structure using the partition function.

1.4. Determine whether nucleotides 3 through 9 of the hammerhead core (**Fig. 1a**) participate in base-pair formation in the dominant OFF state secondary structure using the probability dot matrix plot derived from the partition function. If one or more nucleotides 3 through 9 remain unpaired, reject the sequence and go to 1.1.

1.5. Replace the OBS from the structure with the same number of artificial nucleotides that are defined to have no binding properties.

1.6. Fold the sequence and compute the free energies of this ON state based on the partition function.

1.7. Determine if the resulting dominant structure carries all three stems that are required for function of the hammerhead ribozyme using the probability dot matrix plot derived from the partition function. If there is not such a dominant structure, reject the sequence and go to 1.1.

1.8. Determine the percentage of nucleotides in the OBS that participate in base-pairing interactions in the absence of DNA effector. If this value is <30% or >70%, reject the sequence and go to 1.1.

1.9. Compute the free energy of the dominant OFF state secondary structure based on the partition function and determine the gap between the OFF and ON state free energies. If the energy gap is outside the range −6 and −10 kcal mol^{-1}, reject the sequence and go to 1.1. This gap was chosen based on an estimate of the balance between maintaining a stable OFF state and rapidly overcoming this stability via the energy of DNA effector binding.

1.10. Run the program RNAheat (Vienna RNA folding package) for the ON and OFF states. If the dominant structures are not preserved in the range from 20 to 40 °C, reject sequence and go to 1.1.

1.11. Compute the ensemble diversity for OFF and ON states. If it does not exceed 9 units (higher values indicate greater secondary structure variability)[61], register the sequence as a candidate and go to 1.1. Registered candidates are further processed on an individual basis starting with 2.1.

2.1. Using the secondary structure generated by the stage 1 algorithm wherein the OBS is excluded (see below; parentheses identify base-paired nucleotides), calculate the thermodynamic stability of the structure. Run the program RNAinverse (Vienna RNA folding package) program to generate new RNA sequence that possesses similar secondary structure folding but random sequence of the OBS.

```
(((((((((((((((((((((..(..(((.....)))).
gggcgacccugaugagcuugaguuuXXXXXXXXXXXX
)))))))))))).....(((((....)))))..)))))))))
XXXXXXXXXXaucaggcgaaacggugaaagccguagguugccc
```

2.2. Determine whether nucleotides 3 through 9 of the hammerhead core (**Fig. 1a**) participate in base-pair formation of the dominant secondary structure using the probability matrix derived from the partition function. If one or more nucleotides 3 through 9 remain unpaired, reject the RNA sequence and go to 2.1.

2.3. Compute the thermodynamic stability of the dominant secondary structure provided in step 2.2. If the thermodynamic stability of the structure differs by more than ± 5% compared to the candidate RNA sequence provided in step 1.11, reject the sequence and go to 2.1.

2.4. Compute the thermodynamic stability of the OBS bound to its perfectly matched complement RNA. If the thermodynamic stability of the duplex differs by more than ± 5% compared to the candidate OBS provided in step 1.11, reject the sequence and go to 2.1.

2.5. Run the program RNAheat[61] for the ON and OFF states. If the dominant structures are not preserved in the range from 20 to 40 °C, reject sequence and go to 2.1. The selection of constructs that satisfy this criterion help assure that the RNA switches will function at 23 °C, despite thermodynamic modeling with data established at 37 °C.

2.6. Run the program kinRNA[49] with the RNA sequence derived from stem 2.5. If the dominant structure is not folded within 480 units (larger arbitrary units indicate slower folding), reject sequence and go to 2.1.

2.7. Compute the free energy of the dominant OFF state secondary structure based on the partition function and determine the gap between the OFF and ON state free energies. If the energy gap is more than twofold different than the candidate sequence derived in step 1.11, reject the sequence and go to 2.1.

The procedure applied for the selection of AND, OR and NOT gates utilizes a similar progression of steps. For the AND and OR gates, additional steps were added to compute the structural properties when either one or both effectors are present.

Oligonucleotides. Synthetic DNAs were obtained from Keck Biotechnology Resource Laboratory (Yale University). DNAs were purified by denaturing (8 M urea) PAGE before use. Template DNAs for *in vitro* transcription were prepared by overlap extension using SuperScript II reserve transcriptase (Invitrogen) in a reaction volume of 50 μl according to the manufacturer's instructions. Synthetic DNAs corresponding to the nontemplate strand each carried a T7 RNA promoter sequence (TAATACGACTCACTATA) and 15 nucleotides at the 3′ terminus that overlapped with the synthetic DNA corresponding to the template strand. The resulting double-stranded DNAs were recovered by

precipitation with ethanol and used as templates for transcription *in vitro* (RiboMax; Promega) in the presence of α-^{32}P ATP according to the manufacturer's directions. The transcribed RNAs, produced during a 2-h incubation, were isolated by using denaturing 10% PAGE.

Allosteric ribozyme assays. Radiolabeled RNAs were incubated at 25 °C in a reaction solution containing 100 mM Tris-HCl, (pH 8.3 at 23 °C) and 10 mM $MgCl_2$. NOT-1 ribozyme assays were conducted at 37 °C in a solution containing 2 mM $MgCl_2$, 100 mM KCl, 25 mM NaCl, 50 mM Tris-HCl (pH 7.5 at 37 °C). Ribozyme reactions were initiated by the addition of $MgCl_2$ after pre-incubating NOT-1 and tenfold excess DNA-6 (when present) for 5 min in Mg^{2+}-free reaction buffer. Reactions were terminated by the addition of an equal volume of gel loading buffer containing 200 mM EDTA. The reaction products were analyzed using denaturing 10% or 6% PAGE and the product bands were detected and quantified using a PhosphorImager (Molecular Dynamics). Rate constants were determined by plotting the natural logarithm of the fraction of RNA remaining uncleaved versus time, wherein the negative slope of the resulting line reflects k_{obs}.

Note: Supplementary information is available on the Nature Biotechnology website.

ACKNOWLEDGMENTS

We thank members of the Breaker laboratory for helpful discussions. This work was supported by grants from the National Science Foundation and by the Defense Advance Research Projects Agency (DARPA). This project also was supported in part with Federal funds from the National Heart, Lung, and Blood Institute, National Institutes of Health, under contract No. N01-HV-28186.

COMPETING INTERESTS STATEMENT

The authors declare competing financial interests (see the *Nature Biotechnology* website for details).

Published online at http://www.nature.com/naturebiotechnology/
Reprints and permissions information is available online at http://npg.nature.com/reprintsandpermissions/

1. Breaker, R.R. Natural and engineered oligonucleotides as tools to explore biology. *Nature* **432**, 838–845 (2004).
2. Gold, L., Polisky, B., Uhlenbeck, O.C. & Yarus, M. Diversity of oligonucleotides functions. *Annu. Rev. Biochem.* **64**, 763–797 (1995).
3. Osborne, S.E. & Ellington, A.D. Nucleic acid selection and the challenge of combinatorial chemistry. *Chem. Rev.* **97**, 349–370 (1997).
4. Hamaguchi, N., Ellington, A. & Stanton, M. Aptamer beacons for the detection of proteins. *Anal. Biochem.* **294**, 126–131 (2001).
5. McCauley, T.G., Hamaguchi, N. & Stanton, M. Aptamer-based biosensor arrays for detection and quantification of biological macromolecules. *Anal. Biochem.* **319**, 244–250 (2003).
6. Bock, C. *et al.* Photoaptamer arrays applied to multiplexed proteomic analysis. *Proteomics* **4**, 609–618 (2004).
7. Soukup, G.A. & Breaker, R.R. Nucleic acid molecular switches. *Trends Biotechnol.* **17**, 469–476 (1999).
8. Soukup, G.A. & Breaker, R.R. Allosteric nucleic acid catalysts. *Curr. Opin. Struct. Biol.* **10**, 318–325 (2000).
9. Silverman, S.K. Rube Goldberg goes (ribo)nuclear? Molecular switches and sensors made from RNA. *RNA* **9**, 377–383 (2003).
10. Seetharaman, S., Zivarts, M., Sudarsan, N. & Breaker, R.R. Immobilized RNA switches for the analysis of complex chemical and biological mixtures. *Nat. Biotechnol.* **19**, 336–341 (2001).
11. Hesselberth, J.R., Robertson, M.P., Knudsen, S.M. & Ellington, A.D. Simultaneous detection of diverse analytes with an aptazyme ligase array. *Anal. Biochem.* **312**, 106–112 (2003).
12. Nahvi, A. *et al.* Genetic control by a metabolite binding mRNA. *Chem. Biol.* **9**, 1043–1049 (2002).
13. Winkler, W., Nahvi, A. & Breaker, R.R. Thiamine derivatives bind messenger RNAs directly to regulate bacterial gene expression. *Nature* **419**, 952–956 (2002).
14. Mironov, A.S. *et al.* Sensing small molecules by nascent RNA: a mechanism to control transcription in bacteria. *Cell* **111**, 747–756 (2002).
15. Winkler, W.C., Cohen-Chalamish, S. & Breaker, R.R. An mRNA structure that controls gene expression by binding FMN. *Proc. Natl. Acad. Sci. USA* **99**, 15908–15913 (2002).
16. Sudarsan, N., Barrick, J.E. & Breaker, R.R. Metabolite-binding RNA domains are present in the genes of eukaryotes. *RNA* **9**, 644–647 (2003).
17. Kubodera, T. *et al.* Thiamine-regulated gene expression of *Aspergillus oryzae thiA* requires splicing of the intron containing a riboswitch-like domain in the 5′ UTR. *FEBS Lett.* **555**, 516–520 (2003).
18. Winkler, W.C. & Breaker, R.R. Genetic control by metabolite-binding riboswitches. *ChemBioChem* **4**, 1024–1032 (2003).
19. Vitreschak, A.G., Rodionov, D.A., Mironov, A.A. & Gelfand, M.S. Riboswitches: the oldest mechanism for the regulation of gene expression. *Trends Genet.* **20**, 44–50 (2004).
20. Mandal, M. & Breaker, R.R. Gene regulation by riboswitches. *Nat. Rev. Mol. Cell Biol.* **5**, 451–463 (2004).
21. Lewin, A.S. & Hauswirth, W.W. Ribozyme gene therapy: applications for molecular medicine. *Trends Mol. Med.* **7**, 221–228 (2001).
22. Schubert, S. & Kurreck, J. Ribozyme- and deoxyribozymes-strategies for medical applications. *Curr. Drug Targets* **5**, 667–681 (2004).
23. Werstuck, G. & Green, M.R. Controlling gene expression in living cells through small molecule-RNA interactions. *Science* **282**, 296–298 (1998).
24. Grate, D. & Wilson, C. Inducible regulation of the *S. cerevisiae* cell cycle mediated by an RNA aptamer-ligand complex. *Bioorg. Med. Chem.* **9**, 2565–2570 (2001).
25. Thompson, K.M., Syrett, H.A., Knudsen, S.M. & Ellington, A.D. Group I aptazymes as genetic regulatory switches. *BCM Biotechnol.* **2**, 21 (2002).
26. Suess, B., Fink, B., Berens, C., Stanz, R. & Hillen, W. A theophylline responsive riboswitch based on helix slipping controls gene expression *in vivo*. *Nucleic Acids Res.* **32**, 1610–1614 (2004).
27. Desai, S.K. & Gallivan, J.P. Genetic screens and selections for small molecules based on a synthetic riboswitch that activates protein translation. *J. Am. Chem. Soc.* **126**, 13247–13254 (2004).
28. Breaker, R.R. Engineered allosteric ribozymes as biosensor components. *Curr. Opin. Biotechnol.* **13**, 31–39 (2002).
29. Ferguson, A. *et al.* A novel strategy for selection of allosteric ribozymes yields RiboReporter sensors for caffeine and aspartame. *Nucleic Acids Res.* **32**, 1756–1766 (2004).
30. Srinivasan, J. *et al.* ADP-specific sensors enable universal assay of protein kinase activity. *Chem. Biol.* **11**, 499–508 (2004).
31. Stojanovic, M.N. & Stefanovic, D. Deoxyribozyme-based half-adder. *J. Am. Chem. Soc.* **125**, 6673–6676 (2003).
32. Stojanovic, M. & Stafanovic, D. A deoxyribozyme-based molecular automaton. *Nat. Biotechnol.* **21**, 1069–1074 (2003).
33. Tang, J. & Breaker, R.R. Rational design of allosteric ribozymes. *Chem. Biol.* **4**, 453–459 (1997).
34. Jose, A.M., Soukup, G.A. & Breaker, R.R. Cooperative binding of effectors by an allosteric ribozyme. *Nucleic Acids Res.* **29**, 1631–1637 (2001).
35. Soukup, G.A. & Breaker, R.R. Engineering precision RNA molecular switches. *Proc. Natl. Acad. Sci. USA* **96**, 3584–3589 (1999).
36. Koizumi, M., Kerr, J.K., Soukup, G.A. & Breaker, R.R. Allosteric ribozymes sensitive to the second messengers cAMP and cGMP. *Nat. Struct. Biol.* **6**, 1062–1071 (1999).
37. Robertson, M.P., Knudsen, S.M. & Ellington, A.D. *In vitro* selection of ribozymes dependent on peptides for activity. *RNA* **10**, 114–127 (2004).
38. Porta, H. & Lizardi, P.M. An allosteric hammerhead ribozyme. *Biotechnol.* **13**, 161–164 (1995).
39. Komatsu, Y., Yamashita, S., Kazama, N., Nobuoka, K. & Ohtsuka, E. Constructuion of new ribozymes requiring short regulator oligonucleotides as a cofactor. *J. Mol. Biol.* **299**, 1231–1243 (2000).
40. Burke, D.H., Ozerova, N.D. & Nilsen-Hamilton, M. Allosteric hammerhead ribozyme TRAPs. *Biochemistry* **41**, 6588–6594 (2002).
41. Wickiser, J.K., Cohen-Chalamish, S., Puskarz, I., Sawiki, B., Ward, D.C. & Breaker, R.R. Engineered oligonucleotides-responsive ribozymes that form structures resembling kissing complexes. (in preparation).
42. Stojanovic, M.N., Mitchell, T.E. & Stefanovic, D. Deoxynbozyme-based logic gates. *J. Am. Chem. Soc.* **124**, 3555–3561 (2002).
43. Wang, D.Y., Lai, B.H., Feldman, A.R. & Sen, D. A general approach for the use of oligonucleotides effectors to regulate the catalysis of RNA-cleaving ribozymes and DNAzymes. *Nucleic Acids Res.* **30**, 1735–1742 (2002).
44. McCaskill, J.S. The equilibrium partition function and base pair binding probabilities for RNA secondary structure. *Biopolymers* **29**, 1109–1119 (1990).
45. Bonhoeffer, S., McCaskill, J.S., Stadler, P.F. & Schuster, P. RNA multi-structure landscapes. A study based on temperature dependent partition functions. *Eur. Biophys. J.* **22**, 13–24 (1993).
46. Russell, R. *et al.* Exploring the folding landscape of a structured RNA. *Proc. Natl. Acad. Sci. USA* **99**, 155–160 (2002).
47. Woodson, S.A. Folding mechanisms of group I ribozymes: Role of stability and contact order. *Biochem. Soc. Trans.* **30**, 1166–1169 (2002).
48. Sosnick, T.R. & Pan, T. RNA folding: Models and perspectives. *Curr. Opin. Struct. Biol.* **13**, 309–316 (2003).
49. Flamm, C., Fontana, W., Hofacker, I. & Schuster, P. RNA folding kinetics at elementary step resolution. *RNA* **6**, 325–338 (2000).
50. Flamm, C., Hofacker, I.L., Maurer-Stroh, Stadler, P.F. & Zehl, M.S. Design of multistable RNA molecules. *RNA* **7**, 254–265 (2001).
51. Forster, A.C. & Symons, R.H. Self-cleavage of plus and minus RNAs of a virusoid and a structural model for the active sites. *Cell* **49**, 211–220.
52. Hertel, K.J. *et al.* Numbering system for the hammerhead. *Nucleic Acids Res.* **20**, 3252 (1992).
53. Osborne, E.M., Schaak, J.E. & DeRose, V.J. Characterization of a native hammerhead ribozyme derived from schistosomes. *RNA* **11**, 187–196 (2005).
54. Khvorova, A., Lescoute, A., Westhof, E. & Jayasena, S.D. Sequence elements outside the hammerhead ribozyme catalytic core enable intracellular activity. *Nat. Struct. Biol.* **10**, 708–712 (2003).

55. De la Pena, M., Gago, S. & Flores, R. Peripheral regions of natural hammerhead ribozymes greatly increase their self-cleavage activity. *EMBO J.* **22**, 5561–5570 (2003).
56. Canny, M.D. *et al.* Fast cleavage kinetics of a natural hammerhead ribozyme. *J. Am. Chem. Soc.* **126**, 10848–10849 (2004).
57. Mandal, M. *et al.* A glycine-dependent riboswitch that uses cooperative binding to control gene expression. *Science* **306**, 275–279 (2004).
58. Yen, L. *et al.* Exogenous control of mammalian gene expression through modulation of RNA self-cleavage. *Nature* **431**, 471–476 (2004).
59. Bayer, T.S. & Smolke, C.D. Programmable ligand-controlled riboregulators of eukaryotic gene expression. *Nat. Biotechnol.* **23**, 337–343 (2005).
60. Isaacs, F.J. *et al.* Engineered riboregulators enable post-transcriptional control of gene expression. *Nat. Biotechnol.* **22**, 841–847 (2004).
61. Penchovsky, R. & Ackermann, J. DNA library design for molecular computation. *J. Comput. Biol.* **10**, 215–229 (2003).
62. Mathews, D., Sabina, J., Zucker, M. & Turner, H. Expanded sequence dependence of thermodynamic parameters provides robust prediction of RNA secondary structure. *J. Mol. Biol.* **288**, 911–940 (1999).
63. Hofacker, I.L. *et al.* Fast folding and comparison of RNA secondary structures. *Monatsh. Chem.* **125**, 167–188 (1994).
64. Hofacker, I.L. Vienna RNA secondary structure server. *Nucleic Acids Res.* **31**, 3429–3431 (2003).

(in press) Electropolymerization on Microelectrodes: A Novel Functionalization Technique for Selective Protein and DNA Conjugation

Eric Stern[11], Steven Jay*[1], James Bertram*[1], Benjamin Boese[2], Ilona Kretzschmar[3], Daniel Turner-Evans[4], Carl Dietz[4], David A. LaVan[5], Tadeusz Malinski[6], Tarek Fahmy[1] & Mark A. Reed[4,7]

Yale University, Departments of [1]Biomedical Engineering, [2]Chemical Engineering, [4]Applied Physics, [5]Mechanical Engineering, and [7]Electrical Engineering; PO Box 208248, New Haven, CT 06520, USA

[3]The City College of New York, Department of Chemical Engineering; 138th Street at Convent Avenue, New York, NY 10031, USA

[6]Ohio University, Department of Biochemistry; 350 W. State Street, Athens, OH 45701, USA

Abstract

A critical shortcoming of current surface functionalization schemes is their inability to selectively coat patterned substrates at micron and nanometer scales. This limitation prevents localized deposition of macromolecules at high densities, thereby restricting the versatility of the surface. A new approach for functionalizing lithographically patterned substrates that eliminates the need for alignment and, thus, is scalable to any dimension is reported. We show, for the first time, that electropolymerization of derivatized phenols can functionalize patterned surfaces with amine, aldehyde, and carboxylic acid groups, and demonstrate that these derivatized groups can covalently bind molecular targets, including proteins and DNA. With this approach, electrically conducting and semiconducting materials in any lithographically realizable geometry can be selectively functionalized, allowing for the sequential deposition of a myriad of chemical or biochemical species of interest at high density to a surface with minimal cross-contamination.

Introduction

There is an ever-increasing demand for the selective placement of functional molecules with micron to nanometer accuracy for sensing, assaying, and signaling applications. The key limitation is that current chemical and biochemical deposition schemes have not kept pace with the precision attainable by both traditional lithography[1], and nanotube and nanowire schemes[2,3]. A method that allows selective functionalization of micro- and nano-scale

[1] Author to whom correspondence should be addressed. Email: Eric.Stern@Yale.edu
* These authors contributed equally to this work

electronic devices would enable multiple potential functions at very high densities on a single surface and would have implications in many fields, including DNA and protein microarrays[4,5], nanowire and nanotube sensors[6], lab-on-a-chip platforms[7], drug discovery platforms[8] and drug delivery systems[9].

In order to achieve selective functionalization, we utilize the method of phenol electropolymerization, which has been previously shown to deposit insulating films on Pt wires[10-16], primarily for the development of amperometric and potentiometric sensors. Electropolymerization is a process whereby a conducting[17-20] or insulating[10] film is deposited on a conductive or semiconductive substrate. Two significant advantages of insulating films, such as polyphenols, are that they are considerably thinner due to the self-limiting nature of the polymerization reaction[10,11,17] and that substrates can be coated without affecting their electronic properties. The electropolymerization of tyramine and 4-hydroxybenzaldehyde has been shown to produce insulating films with reactive amines and aldehydes on bulk electrodes[13-16], but the applications of this approach have been severely limited due to the lack of integration with thin film microelectronic technology, which enables simultaneous functionalization of electrodes in large arrays with different molecular species.

In this article we present a new method capable of applying multiple functionalities sequentially to interdigitated microelectrodes without the need for additional alignment steps, and with no detectable cross-contamination. We demonstrate for the first time that modified phenols can be electrodeposited from aqueous solution onto lithographically patterned substrates to produce surfaces with free amine, aldehyde, and carboxylic acid groups capable of conjugating small molecules, proteins, and DNA oligonucelotides. In contrast with present electrochemical-based methods[21-23], the power of the method introduced here is that it offers multiple conjugation chemistries, is not surface specific, is stable in aqueous environments, and is prepared entirely from commercially available chemicals. We additionally use indium tin oxide (ITO) electrodes in this study because ITO is optically transparent and useful for optical or fluorescent imaging applications.

Experimental Section

ITO Patterning. Positive photoresist (Shipley S1813) was spun on ITO slides (8-12 Ω-cm) purchased commercially (Sigma-Aldrich). The resist was patterned by contact photolithography (CAD Art Services transparency mask) and etched with TE-100 tin etchant (Transene).

Electrode Preparation. The reference electrode was fabricated by depositing AgCl on Ag wire (Earnest Fullham, Inc) in an electrochemical cell from a saturated aqueous NaCl solution. The counter electrode is a Pt wire (Earnest Fullham, Inc) and the working electrode was contacted with a Cascade Microprobetip.

Electrodepositions. Tyramine, 4-hydroxybenzaldehyde, and 4-hydroxyphenylacetic acid were purchased at the highest available grade (Sigma-Aldrich) and used without further purification. The modified phenols were dissolved to 50mM in 1X PBS, pH = 7.4, using ultrasonication; fresh solutions were made at least every hour. Electropolymerization depositions on ITO were performed using a Gamry Femtostat by cycling the counter electrode voltage three times from -0.1 to 4V versus the reference electrode at a sweep rate of 100 mV/s. A comparison of depositions performed on bulk and patterned ITO shows that the peak current during deposition scales linearly with working electrode area. Following deposition, samples were washed with PBS and treated with this buffer with stirring for 15 minutes. Comparing depositions on bulk and patterned ITO, it is evident that the electropolymerization peak current scales linearly with working electrode surface area. Electrodepositions from 100mM modified-phenol in 0.1M KOH in methanol were performed for comparison and similar results to those presented were obtained. It is important to note that nucleophilic R groups such as amines must be at least one carbon removed from the phenyl ring, or they will also polymerize and, hence, be rendered inactive[30]. It should also be noted that we have observed functional electropolymerized films created from 3-hydroxybenzaldehyde and 3-hydroxyphenylacetic acid. Though not studied in this work, ketone functionality can also be obtained by the electropolymerization of modified phenols[13].

Thickness determinations. Three thickness measurements were performed on each of five patterned samples, in which one lead had been coated by electrodeposition. These measurements were taken with a Tencor AlphaStep IQ surface profilometer, which has <5 nm step-height resolution. For each measurement three leads were swept, with the coated lead located between two uncoated leads. The step-heights are determined using the packaged software, which calculates the difference between the average height of the lead and that of the base flanking the lead. The step-heights of the unfunctionalized leads are averaged and the thickness of the film is then calculated by subtracting this value from the step-height of the functionalized lead. Of the 15 total measurements, none of which gave negative film thicknesses, four yielded film thicknesses <5 nm, which is below the resolution of the profilometer.

Blocking measurements. The solution for blocking measurements consists of 50mM Fe^{2+}/Fe^{3+} in 0.1M KCl. The blocking measurements were performed by sweeping from -0.5 to 0.5V versus the reference electrode at 500 mV/s ten times; the tenth curve for each measurement is plotted in Fig 1F.

Sample washing. Prior to all conjugation reactions, chips were rinsed three times with 1X PBS and treated with this buffer for 15 min with agitation. Before imaging, each chip was rinsed with deionized water and blown dry with nitrogen gas. It should be noted that this drying procedure displaces the glass chips that fluoresce due to nonspecific binding.

Amine fluorescence conjugation. Samples were reacted with fluorophores (Molecular Probes) at 0.25 mg/mL in a pH=8.5 bicarbonate buffer at room temperature for 1 hr with agitation. The red fluorophore is AlexaFluor 568 succinimidyl ester and the green is AlexaFluor 350 succinimidyl ester.

Aldehyde and carboxylic acid fluorescence conjugation. Samples were reacted with fluorophores at 0.25 mg/mL in a pH=5.5 acetate buffer for 1 hr at room temperature with agitation. The fluorophore used to bind aldehyde was AlexaFluor 488 hydrazide, sodium salt, and that used to bind carboxylic acid was AlexaFluor 568 hydrazide, sodium salt. The amine-coated slide used as a positive control was purchased from BioSlide, Inc.

Amine quantification. Slide surface free amine quantification was performed based on a serially diluted lysine standard run in triplicate; bound o-phthaldialdehyde (Sigma) was excited at 360 nm and the fluorescence was measured at 460 nm.

Amine and aldehyde quenching. Amine-coated samples were treated with 0.1 M sulfo-N-hydroxysuccinimide (NHS) in pH=8.3 bicarbonate for 1 hr at room temperature with agitation for quenching. Aldehyde-coated samples were quenched with 0.1M hydrazine in pH=6.5 acetate buffer for 1 hr at room temperature with agitation.

Carbodiimide couping, antibody binding, and oligonucleotide hybridization. Carboxylic acid groups (either on BSA or bound to ITO) were treated with 0.015M 1-Ethyl-3-(3-dimethylaminopropyl)-carbodiimide (EDC) and 0.03M NHS at pH=5.5 and amine groups were treated with pH=9.5 buffer for 15 mins at room temperature with agitation. The solutions were then combined and left for 1 hr at room temperature with agitation. The final BSA

concentration was 1 mg/mL. It should be noted that NHS and EDC are not required for the amine-aldehyde reaction of the DNA 20-mer conjugation. Antibody binding was performed in 1X PBS at 37°C for 1 hr at a concentration of 100 μg/mL. Oligonucleotide hybridization was performed at a concentration of 50 μM in 1X SCC buffer (pH=7.2) with 0.05% sodium dodecylsufate at room temperature for 30 mins with agitation.

DNA oligonucleotide sequences. The amino-terminated DNA 20-mer sequence was 5'-H_2N-CGCCACTGCGTCACTGCAGG-3' and the fluorescently-labeled sequence was 5'-FAM-CCTGCAGTGACGCAGTGGCG-3' (IDT, Inc).

BSA quantification. The bound BSA concentration was quantified with an absorbance measurement at 562 nm using a micro BCA protein assay kit (Pierce) based on a serially diluted BSA standard run in triplicate.

Results and Discussion

The deposition solution is created by dissolving a substituted phenol in phosphate buffered saline (Fig. 1A). This is subsequently loaded into an electrochemical cell defined by a poly-dimethylsiloxane (PDMS) gasket (Fig. 1B). Voltage is then cycled between the counter and reference electrodes, while current is measured at the working electrode (the patterned surface in Fig. 1B, which fans out to a contact pad that can be accessed and electrically contacted by a microprobe). The insulating surface coating is produced by a free radical polymerization, which has previously been reported to occur at the ortho positions of the ring[12], in which free radicals are generated by the removal of an electron from deprotonated phenyl rings at the working electrode.

The electropolymerization of tyramine at the working electrode, a patterned ITO lead, is evident from the presence of a strong oxidation peak of ~50 μA during the first sweep in the cyclic voltammogram in Fig. 1C (for an electrode of ~1.53×10^5 μm^2, the current density is ~0.29 nA/μm^2). The absence of this peak from subsequent sweeps indicates that tyramine oxidation is non-reversible and self-limiting. Figs. 1D and E show the cyclic voltammograms for the electropolymerizations of 4-benzaldehyde and 4-hydroxyphenylacetic acid, respectively. Film thickness was determined by profilometry to be between < 5 (the resolution of the profilometer) and 30 nm across 15 measurements (three on each of five samples), with an average of 15 ± 6 nm, lower than that reported previously[14]. This variation is expected as film thickness can be tuned by the sweep rate, the extent of the forced voltage, and the

number of sweeps performed to achieve the thinner values desirable for semiconductor sensing applications or thicker values required to prevent metal corrosion without affecting functionalization.

The insulating nature of the films was evaluated by performing blocking measurements with an iron(II)/iron(III) redox couple (Fig. 1F). For comparison, cyclic voltammetry with this solution was first performed on a bare ITO surface and substantial oxidation and reduction peaks due to the conducting substrate are evident. These peaks are not apparent in blocking measurements performed after film deposition, consistent with the deposition of an insulating (polyphenol) film on the working electrode. The residual current present in these sweeps can be attributed mainly to tunneling through the polyphenol film[24].

We first demonstrate the ability of this method to selectively and sequentially functionalize patterned electrodes. A brightfield image of the edge of the lead pattern on a representative substrate (Fig. 2A) shows three 25 μm-wide, electrically isolated and interdigitated "C-shaped" leads that fan out to contact pads (not shown). A PDMS gasket was placed around the leads to create an electrochemical cell (as depicted in Fig. 1B) and the surface of the innermost lead was functionalized with amine groups by tyramine electropolymerization, as described above. The sample was exposed to a red, amine-reactive fluorophore and the fluorescence micrograph in Fig. 2B demonstrates that amines were selectively introduced as a result of the electropolymerization. The inset plot of the fluorescence intensity shows that the amines are solely detectable on the innermost lead. A subsequent tyramine electrodeposition was performed on the middle lead and the sample was treated with the same amine-reactive fluorophore and imaged; both the innermost and middle leads now fluoresce (Fig. 2C). The electropolymerization/fluorescence conjugation was then performed on the outermost lead and the fluorescence micrograph in Fig. 2D shows all leads fluorescing, indicative of the third selective deposition.

For scalability, it is crucial to know the packing density of amine groups on the surface of the electropolymerized film. The presence of amines on bulk ITO substrates was quantified with an o-phthaldialdehyde assay[25]. We found that there were 3.1 ± 0.7 free amines per nm^2, which was in good agreement with the density of amine surfaces formed by closest-packed self-assembled monolayers in the literature[26] and on a commercially available amine-coated slide that was used as a positive control and showed 2.7 ± 0.4 available amines per nm^2.

To demonstrate the versatility and generality of this technique, we derivatized each of the three leads sequentially with different functional groups and then conjugated different moieties onto each group. First, the outermost lead was functionalized with amine (as described previously) and treated with a blue, amine-reactive fluorophore. Second, the innermost electrode was functionalized with aldehyde by 4-hydroxybenzaldehyde electrodeposition, followed by binding of a green, aldehyde-reactive fluorophore. After quenching remaining aldehyde groups with hydrazine, the middle lead was functionalized with carboxylic acid by 4-hydroxyphenylacetic acid electrodeposition. A red, carboxylic acid-reactive fluorophore was subsequently conjugated to the surface and the sample was then imaged; the fluorescence micrograph is shown in Fig. 3A and the localization of each of the three fluorophores is apparent. The fluorescence intensity plot in Fig. 3B demonstrates the absence of cross-functionalization interaction.

A key feature of this approach is the ability to selectively bind targets arrayed on the substrate. To demonstrate this feature, we studied the localization of a protein, bovine serum albumin (BSA), and a DNA oligonucleotide to the functionalized surfaces. Amine and carboxylic acid groups are desirable for protein conjugation[27], while aldehyde and carboxylic acid groups are preferred for DNA binding[28]. A carbodiimide coupling reaction was utilized to conjugate BSA to the central leads of a chip functionalized with amines. The sample was subsequently incubated with chicken α-BSA-FITC (green fluorescence) immunoglobulin G (IgG) antibody and the fluorescence micrograph of the sample is shown in Fig. 4A. A second sample was electrodeposited with poly-4-hydroxyphenylacetic acid on the innermost lead and then subjected to a similar treatment; the fluorescence micrograph is shown in Fig. 4B. The fluorescent intensity in both samples is localized to the functionalized lead, illustrating the conjugation of BSA to the surface and the subsequent BSA-α-BSA-FITC IgG binding. Surface-conjugated BSA density was determined with a bicinchoninic acid (BCA) assay[29] to be 4.2 ± 0.6 molecules per 100 nm^2 on bulk ITO substrates, which is reasonable given the ~25 nm^2 footprint of the protein.

In order to study the binding of DNA oligonucleotides to the electropolymerized surfaces, a third sample was functionalized with carboxylic acid on the outermost and aldehyde on the innermost lead. A 5' amine-terminated DNA 20-mer was conjugated to the surface under similar conditions for BSA conjugation. The sample was subsequently treated with a complementary DNA 20-mer labeled with a 5'-FAM (green fluorescence) and fluorescently imaged (Fig. 4C). Both functionalized leads fluoresce, demonstrating DNA conjugation to each surface and subsequent hybridization with the fluorescent DNA probe.

Conclusion

To our knowledge this is the first demonstration of a selective-coating electrochemical approach that can be successfully tuned to a wide range of functionalizations. We have demonstrated site-specific conjugation of small molecules, proteins, and DNA oligonucleotides to surface amine, aldehyde, and carboxylic acid groups on insulating films electrodeposited on pre-patterned electrodes. With this approach, electrically conducting and semiconducting materials of any lithographic geometry are capable of being selectively functionalized without additional alignment steps. This *in situ* alignment allows for scaling to nanodevices due to the high density of functional groups on the film surface. Thus, the sequential deposition of numerous chemical or biochemical species of interest at high density on a surface with minimal cross-contamination is realizable. This approach has many potential applications, including selective sensor coating, higher density genomic and DNA arraying, lower volume drug discovery and forensic analyses platforms, and selective coatings for patterning micro- and nanoenvironments for lab-on-a-chip and other microfluidic, microchannel, and MEMS applications.

References

1. ITRS Semiconductor Roadmap: http://public.itrs.net/
2. Wang, J. *Electroanal.* **2005**, *17*, 7-14.
3. Law, M.; Goldberger, J.; Yang, P. D. *Ann. Rev. Mat. Res.* **2004**, *34*, 83-122.
4. Schena, M.; Heller, R.A.; Theriault, T.P.; Konrad, K.; Lachenmeier, E.; Davis, R.W. *Trends Biotech.* **1998**, *16*, 301-306.
5. Templin, M.F.; Stoll, D.; Schrenk, M.; Traub, P.C.; Vöhringer, C.F.; Joos, T.O. *Trends Biotech.* **2002**, *20*, 160-166.
6. Cui, Y.; Wei, Q.; Park, H.; Lieber, C. M. *Science* **2001**, *293*, 1289-1292.
7. Gardeniers, J. G. E.; van den Berg, A. *Anal. Bioanal. Chem.* **2004**, *378*, 1700-1703.
8. Neefjes, J.; Dantuma, N. P. *Nat. Rev. Drug Disc.* **2004**, *3*, 58-69.
9. LaVan, D. A.; McGuire, T.; Langer, R. *Nat. Biotech.* **2003**, *21*, 1184-1191.
10. Bruno, F.; Pham, M.C.; DuBois, J.E. *Electrochim. Acta* **1997**, *22*, 451-457.
11. Eddy, S.; Warriner, K.; Christie, I.; Ashworth, D.; Purkiss, C.; Vadgama, P. *Biosens. Bioelectron.* **1995**, *10*, 831-839.
12. Long, D.D.; Marx, K.A.; Zhou, T. *J. Electroanal. Chem.* **2001**, *501*, 107-113.
13. Pham, M.C.; DuBois, J.-E.; Lacaze, P.-C. *J. Electroanal. Chem.* **1979**, *99*, 331-340.
14. DuBois, J.-E.; Lacaze, P.-C.; Pham, M. C. *J. Electroanal. Chem.* **1981**, *117*, 233-241.
15. Situmorang, M.; Gooding, J.J.; Hibbert, D.B.; Barnett, D. *Biosens. Bioelec.* **1998**, *13*, 953-962.
16. Situmorang, M.; Gooding, J.J.; Hibbert, D.B. *Anal. Chim. Acta.* **1999**, *394*, 211-223.
17. Yousaf, M.N.; Mrksich, M. *J. Am. Chem. Soc.* **1999**, *121*, 4286-4287.
18. Curreli, M.; Li, C.; Sun, Y.; Lei, B.; Gundersen, M.A.; Thompson, M.E.; Zhou, C. *J. Am. Chem. Soc.* **2005**, *127*, 6922-6923.
19. Bunimovich, Y.L.; Ge, G.; Beverly, K.C.; Ries, R.S.; Hood, L.; Heath, J.R. *Langmuir* **2004**, *20*, 10630-10638.
20. Bartlett, P.N.; Cooper, J.M. *J. Electroanal. Chem.* **1993**, *362*, 1-12.
21. Konry, T.; Novoa, A.; Cosnier, S.; Marks, R.S. *Anal. Chem.* **2003**, *75*, 2633-2639.
22. Cosnier, S. *Anal. Bioanal. Chem.* **2003**, *377*, 507-520.
23. Adamcova, Z.; Ludmila, D. *Prog. Org. Coat.* **1989**, *16*, 295-320.

24. Gao, Z.; Siow, K.S. *Electrochim. Acta* **1997**, *42*, 315-321.

25. Buck, R.H.; Krummen, K. *J. Chromatogr.* **1987**, *387*, 255-265.

26. Lateef, S.S.; Boateng, S.; Ahluwalia, N.; Hartman, T.J.; Russell, B.; Hanley, L. *J. Biomed. Mat. Res. A* **2005**, *72A*, 373-380.

27. Hermanson, G.T. *Bioconjugate Techniques*; Academic Press: New York; 1996.

28. Taylor, S.; Smith, S.; Windle, B.; Guiseppi-Elie, A. *Nucl. Acid. Res.* **2003**, *31*, e87.

29. Smith, P.K.; Krohn, R.I.; Hermanson, G.T.; Mallia, A.K.; Gartner, F.H.; Provenzano, M.D.; Fujimoto, E.K.; Goeke, N.M.; Olson, B.J.; Klenk, D.C. *Anal. Biochem.* **1985**, *150*, 76-85.

30. Guenbour, A.; Kacemi, A.; Benbachir, A. *Prog. Org. Coat.* **2000**, *39*, 151-155.

Acknowledgements

The authors would like to thank James Klemic for many helpful discussions and assistance with manuscript preparation; Alec Flyer, Pauline Wyrembak, Elnaz Menhaji, and Kathryn Klemic for many helpful discussions and experimental suggestions, David Stern for help preparing the manuscript; Millicent Ford for assistance with fluorescence microscopy; Menno de Jong for assistance designing the electrochemical cell; Russel, Nicholas, and Vincent Bernando for help with the design and machining of the electrochemical cell; and Fred Sigworth, Ron Breaker, Mark Saltzman, and Erin Lavik for helpful discussions about fluorescence detection. This work was partially supported by DARPA through AFOSR, ARO (DAAD19-01-1-0592), AFOSR (F49620-01-1-0358), NASA (NCC 2-1363), by a Department of Homeland Security graduate fellowship, and by a NSF graduate fellowship.

Figure Captions

Figure 1. A. Schematic of surface electrochemical polymerization. R=$(CH_2)_2NH_2$, CHO, CH_2COOH for tyramine, 4-hydroxybenzaldehyde, and 4-hydroxyphenylacetic acid, respectively; B. Schematic (not to scale) of an electrochemical cell defined by a PDMS gasket on a patterned ITO-on-glass substrate; C. Cyclic voltammogram of the electropolymerization of tyramine (inset) on a single patterned ITO lead on a glass substrate (Fig. 1B). The potential at which the oxidation occurs is strongly dependent on (i) the working electrode material and (ii) the freshness of the reference electrode (the peak has been seen to occur between ~2.4-3.25V on ITO); D. Cyclic voltammogram of 4-hydroxybenzaldehyde (inset) elctrodeposition on a patterned ITO lead; E. Cyclic voltammogram of 4-hydroxyphenylacetic acid (inset) electrodeposition on a patterned ITO lead; F. Cyclic voltammogram of the blocking solution on bare ITO, polytyramine-coated ITO (NH_2), poly-4-hydroxybenzaldehyde-coated ITO (CHO), and poly-4-hydroxyphenylacetic acid-coated ITO (COOH). The measurements were taken with the same cell used for deposition. The reduction and oxidation peaks are not symmetric about 0V due to coating of the reference electrode. All experiments were repeated over twenty times with similar results.

Figure 2. A. A bright field image showing the three parallel "C-shaped" ITO leads. Treatment with a red, amine-reactive fluorophore and subsequent fluorescence imaging at this stage (TRITC filter) showed no specific binding (not shown); B. Fluorescence image (TRITC filter) of the chip shown in A with the inner lead coated with polytyramine and subsequently reacted with a red amine-reactive fluorophore. The inset plot shows the fluorescence intensity (determined with arbitrary units defined by ImageJ) versus distance for the orange cutline. Leads functionalized with amines and subsequently quenched exhibited no specific fluorescence pattern when treated with the same fluorophore; C. Fluorescence image (TRITC filter) of the chip shown in B with the middle lead now coated with polytyramine and a subsequent reaction with the same dye. Visible scratches were purposely introduced at this stage (with tweezers) to register sample identity; D. Same as C but with the outermost lead also coated with polytyramine and reacted with the same dye. The scratch patterns in C and D are identical. The white scale bar in all images represents 100 μm. The experiment was repeated four times with similar results. The average intensity of the fluorescent signal across the 25-μm leads for the four experiments was 37 ± 4 over a background of 8 ± 5.

Figure 3. A. Multiple-fluorescence (DAPI, GFP, and TRITC filters) image of a central part of the lead pattern for a sample treated as follows: polytyramine was deposited on the outermost lead and the chip was subsequently treated with a blue, amine-reactive fluorophore. Poly-4-hydroxybenzene was then deposited on the innermost lead, followed by chip treatment with a green, aldehyde-reactive fluorophore. Free aldehyde groups were then quenched. Lastly, poly-4-hydroxyphenylacetic acid was deposited on the middle lead and the chip was treated a red, carboxylic acid-reactive fluorophore. The scale bar represents 100 μm; B. Fluorescence intensity versus position for the red cutline in A. The line color corresponds to the fluorescence color in Fig 3A; the fluorescence intensity units are defined by ImageJ. The experiment was repeated three times with similar results.

Figure 4. A. Fluorescence micrograph of the end of an electrode pattern first coated with polytyramine, then carbodiimide coupled to BSA, and lastly incubated with a fluorescently-labeled BSA IgG, as illustrated by the schematic inset. The "bottom view" is immunofluorescence viewed through the ITO; the "top view" is the immunofluorescence viewed directly, illustrating the transparency of ITO. When the α-BSA IgG was replaced with a nonimmune, fluorescently labeled IgG from the same species and at the same concentration, or when BSA was not bound on the surface prior to α-BSA-FITC IgG incubation, no specific immunofluorescence pattern was observed (not shown); B. Fluorescence micrograph of the lead pattern with the innermost lead first coated with poly-4-hydroxyphenylacetic acid and then treated as in panel A (schematic inset); C. Fluorescence micrograph of a patterned substrate coated with poly-4-hydroxybenzaldehyde on the innermost leads and poly-4-hydroxyphenylacetic acid on the outermost leads. Subsequently, carbodiimide coupling was performed to an amino-terminated DNA 20-mer, followed by hybridization using a fluorescently labeled complementary 20-mer and subsequent fluorescence imaging. When a noncomplementary DNA 20-mer was used for hybridization at the same concentration or when DNA was not immobilized on the lead surface prior to probe hybridization, no specific fluorescence was observed (not shown). All fluorescent images were taken with a GFP filter and the scale bar in each micrograph represents 100 μm. All experiments were repeated four times with similar results.

Figure 1

A:

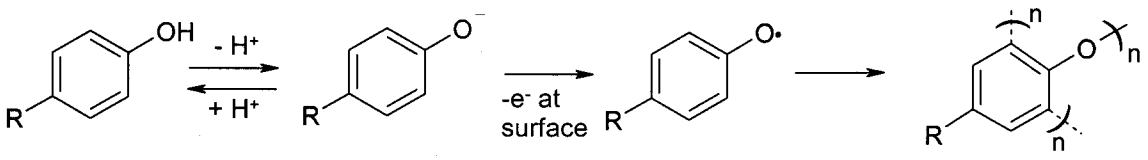

B

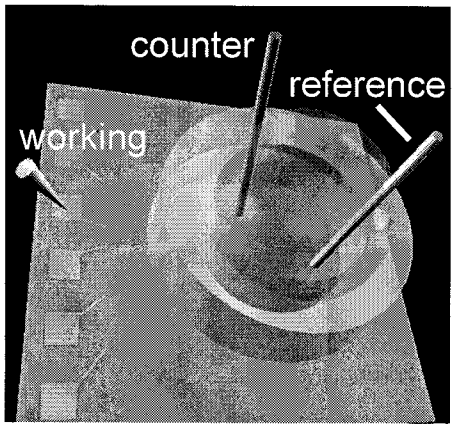

C

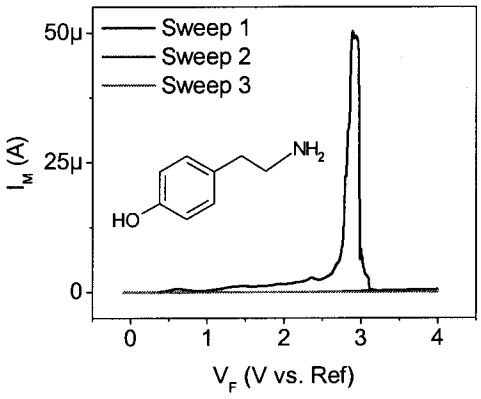

D

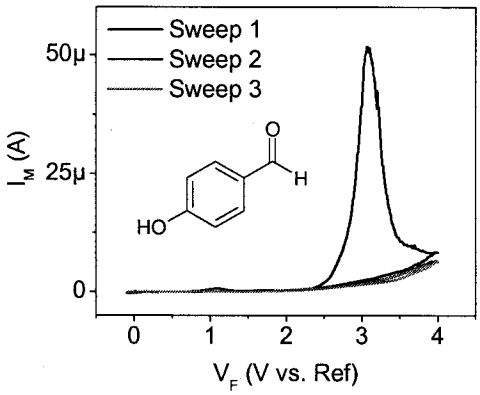

E

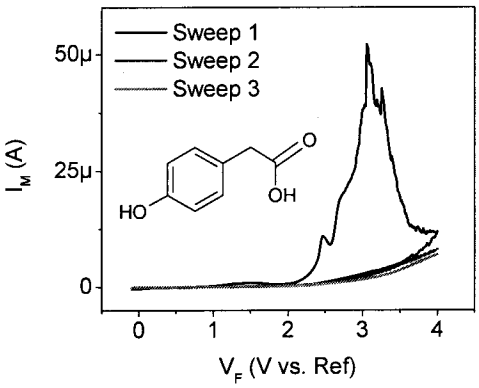

F

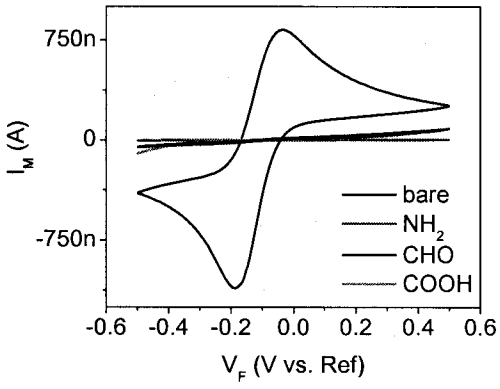

Figure 2

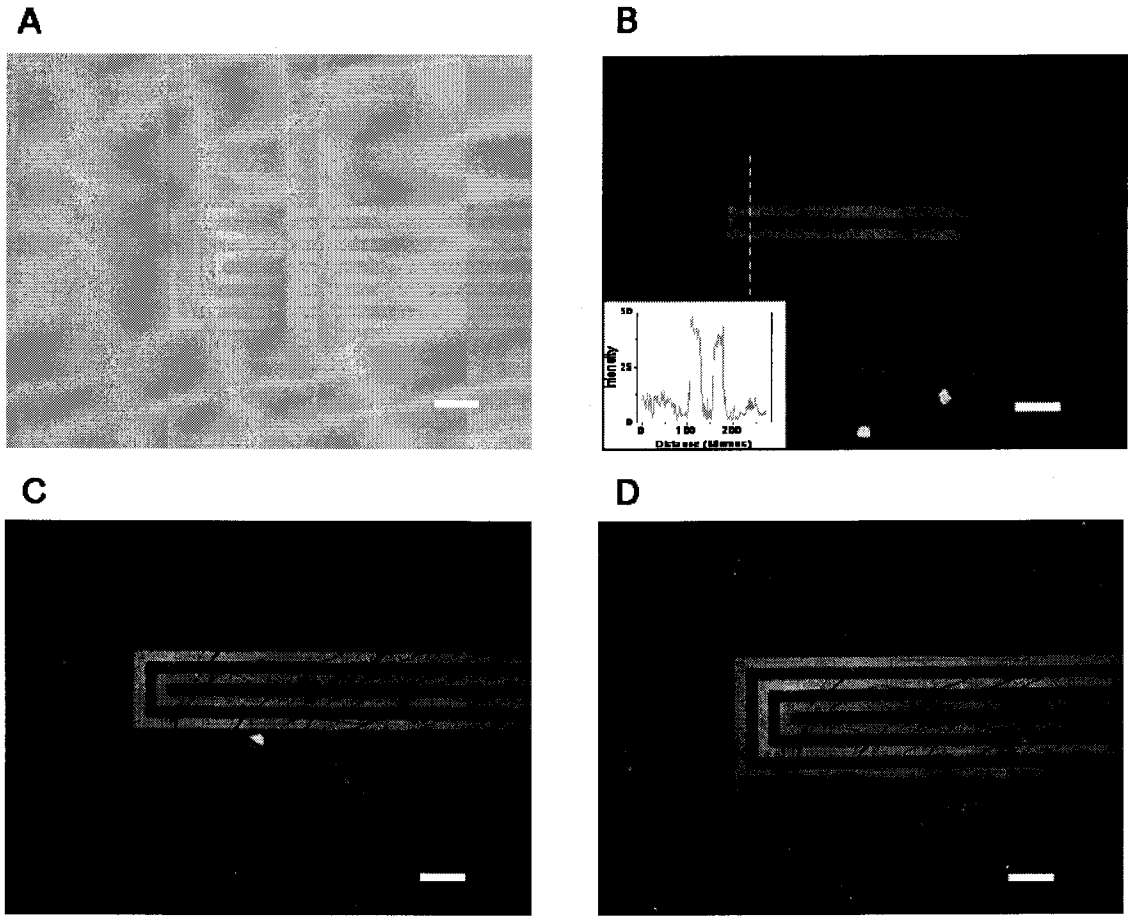

Figure 3

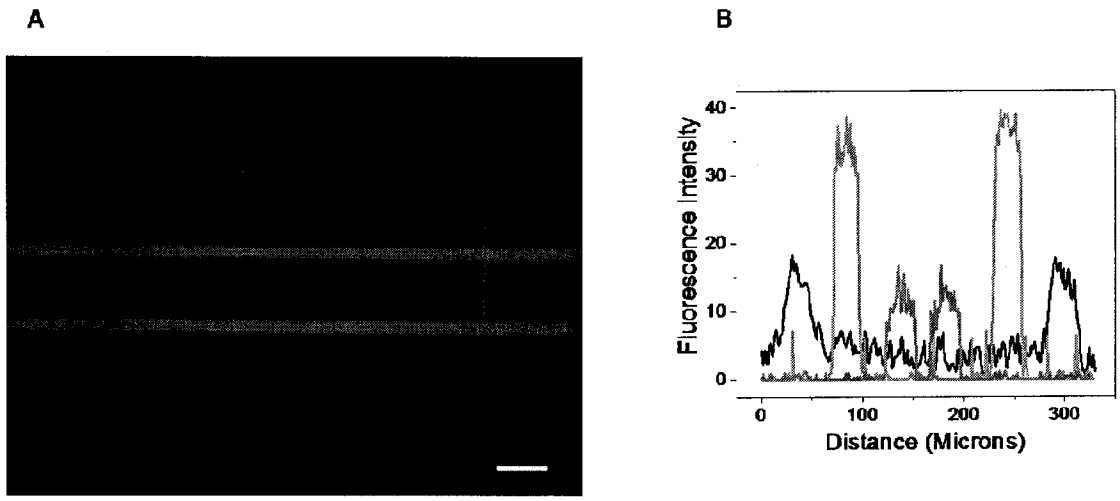
A
B
Fluorescence Intensity
40
30
20
10
0
0
100
200
300
Distance (Microns)

Figure 4

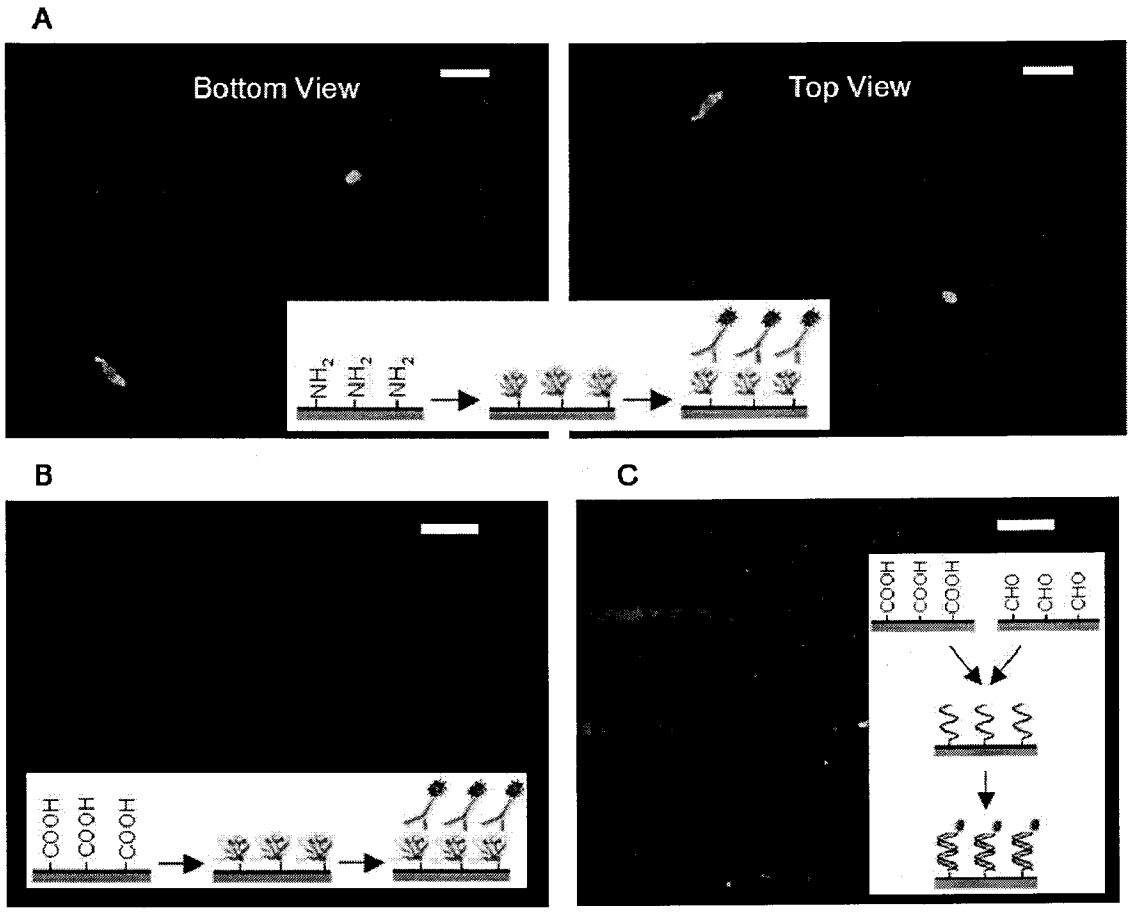
A
Bottom View
Top View
NH2
NH2
NH2
B
COOH
COOH
COOH
C
COOH
COOH
COOH
CHO
CHO
CHO